© 2022. Published by The Company of Biologists Ltd | Development (2022) 149, dev201012. doi:10.1242/dev.201012

RESEARCH ARTICLE

FGF8 induces chemokinesis and regulates condensation of mouse nephron progenitor cells

Abhishek Sharma[1,2,*], Marco Meer[3,4,*], Arvydas Dapkunas[5], Anneliis Ihermann-Hella[5], Satu Kuure[5,6], Seppo J. Vainio[1,2,7,8,9,‡], Dagmar Iber[3,4,‡] and Florence Naillat[1,2,‡]

ABSTRACT

Kidneys develop via iterative branching of the ureteric epithelial tree and subsequent nephrogenesis at the branch points. Nephrons form in the cap mesenchyme as the metanephric mesenchyme (MM) condenses around the epithelial ureteric buds (UBs). Previous work has demonstrated that FGF8 is important for the survival of nephron progenitor cells (NPCs), and early deletion of *Fgf8* leads to the cessation of nephron formation, which results in post-natal lethality. We now reveal a previously unreported function of FGF8. By combining transgenic mouse models, quantitative imaging assays and data-driven computational modelling, we show that FGF8 has a strong chemokinetic effect and that this chemokinetic effect is important for the condensation of NPCs to the UB. The computational model shows that the motility must be lower close to the UB to achieve NPC attachment. We conclude that the FGF8 signalling pathway is crucial for the coordination of NPC condensation at the UB. Chemokinetic effects have also been described for other FGFs and may be generally important for the formation of mesenchymal condensates.

KEY WORDS: Computing modelling, Condensation step, Kidney development, Nephron progenitor cells

INTRODUCTION

Mesenchymal condensation is an essential step in kidney development for the early formation of nephrons. This mechanism consists of reciprocal interactive signalling between mesenchymal cells and their surroundings, the epithelial and stromal cells (Das et al., 2013; O'Brien, 2019; Oxburgh, 2018). In addition to reciprocal signalling, intercellular interactions, cellular morphogenesis, i.e. apoptosis or adhesion, and cell migration play an essential role during the establishment of mesenchymal condensation (Ribatti and Santoiemma, 2014; Scarpa and Mayor, 2016; SenGupta et al., 2021). Cell migration can be influenced by chemical, thermal, galvanic, electrical, gravitational or mechanical stimuli, or combinations of these phenomena. A stimulus can cause a tactic response, in which cell movement is directed to the location of the stimulus, or a kinetic response, i.e. random locomotion, in which the magnitude of the response depends on the intensity of the stimulus (Diehn et al., 1977). Particularly in the presence of chemical gradients, cells can show strong chemotactic or chemokinetic responses.

In mice, around embryonic day (E) 11-11.5, mesenchymal condensation in the nephrogenic niche of the developing kidney results in the formation of the cap mesenchyme (CM) (O'Brien, 2019; Davies, 2016). At the same time, nephron progenitor cells (NPCs) from the CM migrate in a stochastic fashion between the top (or tip region) of the epithelial ureteric bud (UB) and the bottom (or trunk region) (Fig. 1) (Combes et al., 2016; Lindström et al., 2018a; Lawlor et al., 2019). NPC fate is niche region specific and requires reciprocal signals between the UB and the surrounding mesenchymal and stromal cells (Fig. 1) (Das et al., 2013; O'Brien, 2019; Lawlor et al., 2019; Carroll et al., 2005; Reginensi et al., 2013; Brown et al., 2013; O'Brien et al., 2018; Li et al., 2021). NPCs that are located in the tip region of the UB maintain their progenitor state and are thus called true nephron progenitor cells (tNPCs) (Fig. 1) (Lindström et al., 2018a,b; Brown et al., 2013). NPCs that migrate downwards to the trunk region are further primed by factors from the UB, becoming committed NPCs (cNPCs) (O'Brien, 2019; Carroll et al., 2005; Brown et al., 2013; O'Brien et al., 2018). A fraction of the cNPCs in the trunk region starts to form a pretubular aggregate (PTA), initiating nephron formation (O'Brien, 2019; Combes et al., 2016; Lawlor et al., 2019; Carroll et al., 2005; Stark et al., 1994). The regulation of NPC fates, migration and priming have been studied intensely (O'Brien, 2019; Oxburgh, 2018; Mari and Winyard, 2015), but the mechanism underlying the condensation of NPCs to the UB is not yet understood. Various signalling factors, receptors and extracellular matrix molecules have been suggested to play a role in NPC condensation (Fig. 1), but its key regulators remain elusive (Combes et al., 2016; Trueb, 2011; Mathew et al., 2012; Kuure and Sariola, 2020).

Fibroblast growth factors (FGFs) are a family of signalling proteins that govern different aspects of kidney development, including UB branching and maintenance of NPCs (Walker et al., 2016). Deletion or mutations in either FGFs or their receptors (FGFRs) can lead to either kidney agenesis or disorders (Walker et al., 2016). FGF8 is expressed in the mesenchyme and is required for both the regulation of downstream genes involved in PTA formation and cell survival (Carroll et al., 2005; Perantoni et al., 2005; Grieshammer et al., 2005; Huh et al., 2020). Deletion of *Fgf8* from kidney primordia leads to a lack of mature nephrons, and eventually to lethality within 24 h of birth (Perantoni et al., 2005).

[1]Faculty of Biochemistry and Molecular Medicine, University of Oulu, Oulu 90220, Finland. [2]Biocenter Oulu, Oulu 90220, Finland. [3]Department of Biosystems, Science and Engineering, ETH Zürich, Zürich 04058, Switzerland. [4]Swiss Institute of Bioinformatics, Lausanne 1015, Switzerland. [5]HiLIFE and Research Programs Unit, Faculty of Medicine, University of Helsinki, Helsinki 00014, Finland. [6]GM-Unit, LAC/HiLIFE, and Medicum, University of Helsinki, Helsinki 00014, Finland. [7]Infotech Oulu, Oulu 90200, Finland. [8]Borealis Biobank, Oulu 90200, Finland. [9]Kvantum Institute, University of Oulu, Oulu 90200, Finland.
*These authors contributed equally to this work

‡Authors for correspondence (florence.naillat@oulu.fi; dagmar.iber@bsse.ethz.ch; seppo.vainio@oulu.fi)

A.S., 0000-0003-0065-412X; M.M., 0000-0003-4501-6121; A.D., 0000-0002-0699-1808; S.K., 0000-0002-9076-0622; S.J.V., 0000-0001-9319-3566; D.I., 0000-0001-8051-1035; F.N., 0000-0003-3061-4460

Handling Editor: Steve Wilson
Received 8 June 2022; Accepted 23 September 2022

Development (2022) 149, dev201012. doi:10.1242/dev.201012

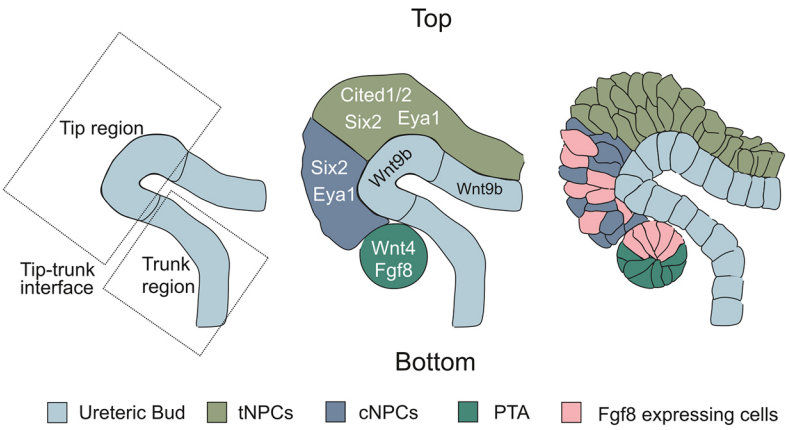

Fig. 1. The UB and the CM nephron progenitor population during early kidney development. True NPCs (tNPCs) express *Cited1*, *Cited2*, *Six2* and *Eya1*, while committed NPCs (cNPCs) lose *Cited1* and *Cited2* expression upon priming by Wnt9b from the UB. A subset of cNPCs continues to form a pretubular aggregate (PTA) at the tip-trunk interface. Gene information taken from Lindström et al. (2018a,b) and Mugford et al. (2009).

The failure of nephron maturation has been attributed to the lack of expression of *Wnt4* and *Lim1* (*Lhx1*), both of which are crucial for mesenchymal-epithelial transition (MET) (Perantoni et al., 2005). However, culturing isolated MM cells from kidneys lacking *Fgf8* along with a WNT source (embryonic spinal cord) failed to initiate nephrogenesis (Perantoni et al., 2005; Grieshammer et al., 2005), supporting the notion that WNT4 and FGF8 work independently. Furthermore, when ectopic FGF8 was added in combination with a WNT source, MMs lacking *Fgf8* expression formed PTAs (Perantoni et al., 2005). These results indicate that FGF8 enhances WNT4 expression in PTAs but also suggest that FGF8 and WNT4 work independently. Because little is known about the specific role of FGF8 during cap mesenchyme formation, we further characterize its function and show that FGF8 signalling co-regulates both NPC migration and mesenchymal condensation.

RESULTS

Without the expression of *Fgf8*, cap mesenchyme formation and attachment of CM cells to the UB are impaired

When the kidney develops from the posterior intermediate mesoderm (Costantini and Kopan, 2010), the brachyury/*T* gene is required for the formation of the posterior mesoderm and axial development (Clements et al., 1996). Hence, brachyury/T^{Cre}-mediated deletion leads to the deletion of *Fgf8* in both epithelial and mesenchymal compartments of the developing kidney (Perantoni et al., 2005; Costantini and Kopan, 2010; Clements et al., 1996). To examine more closely the involvement of FGF8 in kidney development, we stained mutant kidneys ($Fgf8^{n/c}$;T^{Cre}) with SIX2, a known NPC marker (O'Brien, 2019; Oxburgh, 2018).

In $Fgf8^{n/c}$;T^{Cre} mutant kidneys, we found that the $Six2^{+}$ cell population was diminished and less condensed than in the controls (Fig. 2A,B). The reduced cell number has previously been attributed to increased cell death in *Fgf8*-deficient kidneys (Perantoni et al., 2005). We hypothesized that the absence of FGF8 signalling additionally leads to decreased cell motility and consequent failure of mesenchymal condensation, and eventually to the termination of nephrogenesis. To test this hypothesis, we first investigated whether the failure of $Six2^{+}$ cells to condensate would also occur in an *in vitro* culture assay. We used the Trowell culture method to culture $Fgf8^{n/c}$;T^{Cre} kidneys and littermate control kidneys. After 3 days of culture, corresponding to E16.5, we found that the $Six2^{+}$ cells in mutant kidneys were significantly less condensed when compared with their littermate controls (Fig. 2C,D).

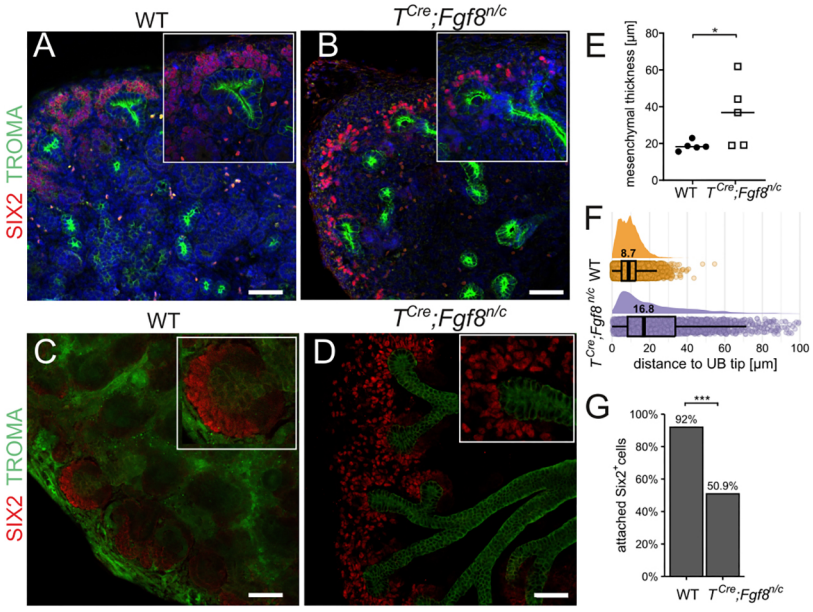

Fig. 2. Impaired cap mesenchyme formation. (A-D) Kidneys were stained for SIX2 (NPCs, red) and TROMA (UB, green), and DNA was counterstained with Hoechst 33342 (blue). Scale bars: 100 µm. (A) E16.5 littermate control. (B) E16.5 kidneys where *Fgf8* was deleted using T^{Cre}. (C) Littermate control E11.5 kidneys cultured in the Trowell culture system. (D) E11.5 kidneys where *Fgf8* was deleted using T^{Cre} cultured in the Trowell system. (B,D) NPCs did not form a condensed cap mesenchyme, but were scattered around the tip region of the UB when compared with the littermate controls (A,C). The insets show areas at higher magnification. (E) Cap mesenchymal thickness as the distance of the last layer of $Six2^{+}$ cells from the UB tip of cultured E11.5 $Fgf8^{n/c}$;T^{Cre} kidneys. *P<0.05 (unpaired *t*-test followed by the Mann–Whitney test; n=5). (F) Distributions of distances between the centroids of $Six2^{+}$ cells and the UB tip in E16.5 Trowell-cultured $Fgf8^{n/c}$;T^{Cre} kidneys (n=13) and littermate controls (n=15) (pooled data). Numbers above the boxplots represent median distances. (G) Percentage of $Six2^{+}$ cells attached to the UB for wild-type control kidneys and $Fgf8^{n/c}$;T^{Cre} mutant kidneys. $Six2^{+}$ cells were classified as being attached to the UB when their centroid position was within a distance of 17.4 µm from the UB, corresponding to twice the median position of $Six2^{+}$ cells in the controls. Sample size n and total number of cells N (pooled): control kidneys (n=7, N=11,425), mutant kidneys (n=8, N=3214). ***P<0.001 (Wilcoxon signed-rank test).

Development (2022) 149, dev201012. doi:10.1242/dev.201012

More specifically, we found that the CM in mutant kidneys was on average twice as thick as in the controls (Fig. 2E). In accordance with this observation, the *Six2*$^+$ cells in mutant kidneys were strongly dispersed within the niche (Fig. 2F). We therefore wondered whether the number of *Six2*$^+$ cells that are attached to the UB was also affected as a result. Attachment to the UB has previously been suggested to affect the differentiation capacity of mesenchymal cells (O'Brien et al., 2018). We classified *Six2*$^+$ cells as being attached to the UB when their centroid position was closer to the UB tip than a threshold value of 17.4 µm, which corresponds to twice the median position of *Six2*$^+$ cells that we measured in the controls (Fig. 2F). Our choice of threshold value agrees well with the upper quartile of distances that were previously ascribed to the attached state (15.2 µm; Combes et al., 2016). We also found that the percentage of attached cells in our controls (92%, Fig. 2G) was in good agreement with what was previously found (85%, compare with Combes et al., 2016). Finally, we found that in our *Fgf8*-deficient mutant kidneys, the proportion of *Six2*$^+$ cells that was attached to the UB tip was significantly lower than in the controls (Fig. 2G). Thus, as a next step, we wanted to investigate the effect of FGF8 on the *Six2*$^+$ NPC population in more detail.

FGF8 induces NPC aggregate formation *in vitro* and is required for tNPC maintenance

The *Six2*$^+$ NPCs dominate the CM population around the UB (Brunskill et al., 2014), and when these cells are primed as cNPCs, a subset of these cNPCs forms a PTA (O'Brien, 2019; Oxburgh, 2018). In an exhaustive study of secreted FGF family members that are required for the maintenance of the tNPC state, it has been suggested that FGF8 fails to maintain the true progenitor state of NPCs (Brown et al., 2011). However, this study made use of a 2D monolayer culture, which differs from the 3D *in vivo* microenvironment of the developing kidney. Ihermann-Hella et al. and Dapkunas et al. have since developed a 3D culture system for NPCs (Ihermann-Hella et al., 2018; Dapkunas et al., 2019). Much as in the 2D cultures, MM cells form aggregates when cultured with FGF2 in the 3D cultures (Ihermann-Hella et al., 2018; Perantoni et al., 1995). To test whether NPCs would also condense in response to FGF8, we cultured the dissociated NPCs from E11.5 kidneys in a 3D matrix along with FGF2 (positive control), FGF8 or anti-FGF8 antibody to block any FGF8 secreted by MM cells. The chosen monoclonal anti-FGF8 antibody binds selectively to FGF8 in *in vitro* experiments (Fig. S1). From dissected E11.5 kidneys, MM was separated from the UB, dissociated into single cell suspension, seeded in Matrigel and cultured for 24 h.

In response to both FGF2 and FGF8, the NPCs formed condensates and retained *Six2* expression (Fig. 3B,C), while both the control and NPCs treated with anti-FGF8 antibody lost *Six2* expression (Fig. 3A,D; Movie 1). To confirm that the NPC population that is positive for SIX2 is also expressing another early marker for condensation, we looked at PAX2, which is a marker for progenitors and early nephron precursors (Dapkunas et al., 2019). Anti-PAX2 antibody stained the NPC condensates in the presence of FGF8 ligand but no staining was observed in the condensates without FGF8 ligand or with anti-FGF8 antibody (Fig. 3F-H). As previously reported by Grieshammer et al. (2005), the absence of FGF8 leads to cell death; a similar observation was made in nephrospheres lacking FGF8 when compared with ectopic FGF8 nephrosphere assays, and a similar result is observed for the live cell number (Fig. 3E). This suggests that FGF8 plays an additional role in NPC commitment along with its role in the formation of NPC condensates. To examine the differentiation stage of NPCs between tNPCs and cNPCs, a qPCR analysis of NPCs in the presence or absence of FGF8 was carried out. tNPC markers such as *Cited2*, *Six2* and *Eya1* were maintained by ectopic FGF8 (Fig. 3I). To confirm that the results were not influenced by signals from the UB, the same experiment was carried out with fully dissociated MMs lacking UB. Similar results were obtained with retained tNPC markers when treated with ectopic FGF8 (Fig. 3J). It has been reported that crosstalk between WNT and FGF signalling pathways is linked by modulation of phosphorylation of *Gsk3b* (Katoh and Katoh, 2006), but we did not observe this in our setting (Fig. S2). Finally, in wild-type kidneys that were cultured in the presence of ectopic FGF8 (Trowell culture method), we observed an expansion of the *Six2*$^+$ population (Fig. 3K). In conclusion, our 3D culture matrix experiments suggest that FGF8 is required for both NPC condensation and tNPC maintenance.

FGF8 elicits a chemokinetic response

FGFs have been shown to act as chemoattractants that trigger a chemotactic response (Makarenkova et al., 2009; Bae et al., 2012), i.e. the migration of a cell along the concentration gradient of the chemoattractant. To determine how FGF8 affects NPC motility, we placed a FGF8-soaked bead in a 3D Matrigel matrix containing MM cells from E11.5 kidneys and tracked cells (Movie 2). Cell tracking revealed that MM cells migrated significantly faster compared with the control bead experiments, but cellular motion was stochastic and lacked directionality (Fig. 4; Movie 2). This shows that FGF8 has mainly a chemokinetic effect, i.e. an impact on the speed of movement, rather than a chemotactic effect.

Here, we note that we did not measure the FGF8 concentration profile and thus cannot exclude the possibility that meaningful gradients did not emerge due to rapid dispersion of FGF8 in Matrigel. Previous measurements in zebrafish showed that the diffusion coefficient of FGF8 is high in aqueous environments (Yu et al., 2009). However, a slow-moving fraction of FGF8 with a reduced diffusion coefficient has been shown to persist due to interactions with heparan sulphate proteoglycans (HSPGs), which are also present in Matrigel and have been shown to play a crucial role in the extracellular distribution of growth factors, modulating morphogen signalling and transport (Makarenkova et al., 2009; Yan and Lin, 2009; Matsuo and Kimura-Yoshida, 2014; Stapornwongkul and Vincent, 2021; Krishnan Harish et al., 2022 preprint).

Ultimately, we find that the measured cell speeds in our FGF8 bead assays (4.6±0.5 µm/h; Fig. 4N) are comparable with those measured by others in the UB tip region (Combes et al., 2016; Tikka et al., 2022). Interestingly, in the presence of FGF8-soaked beads, most cells formed large aggregates, resulting in a collective movement resembling swarm behaviour, which is reflected in the bifurcation of the track straightness measurements of FGF8 versus control (Fig. 4E,F; Movie 2). In the control bead experiments, only a few small aggregates were formed, presumably owing to low levels of *Fgf8* expression by some MM cells.

In summary, we find that FGF8 triggers a chemokinetic response of MM cells from E11.5 kidneys. This observation of undirected cellular motility agrees with previous quantifications where MM cells were found to move semi-stochastically and in a swarming-like manner (Combes et al., 2016).

A model based on FGF8-induced motility leads to robust condensation of NPCs

We next decided to test the impact of FGF8-induced chemokinesis on NPC condensations at the UB using computational modelling.

Development (2022) 149, dev201012. doi:10.1242/dev.201012

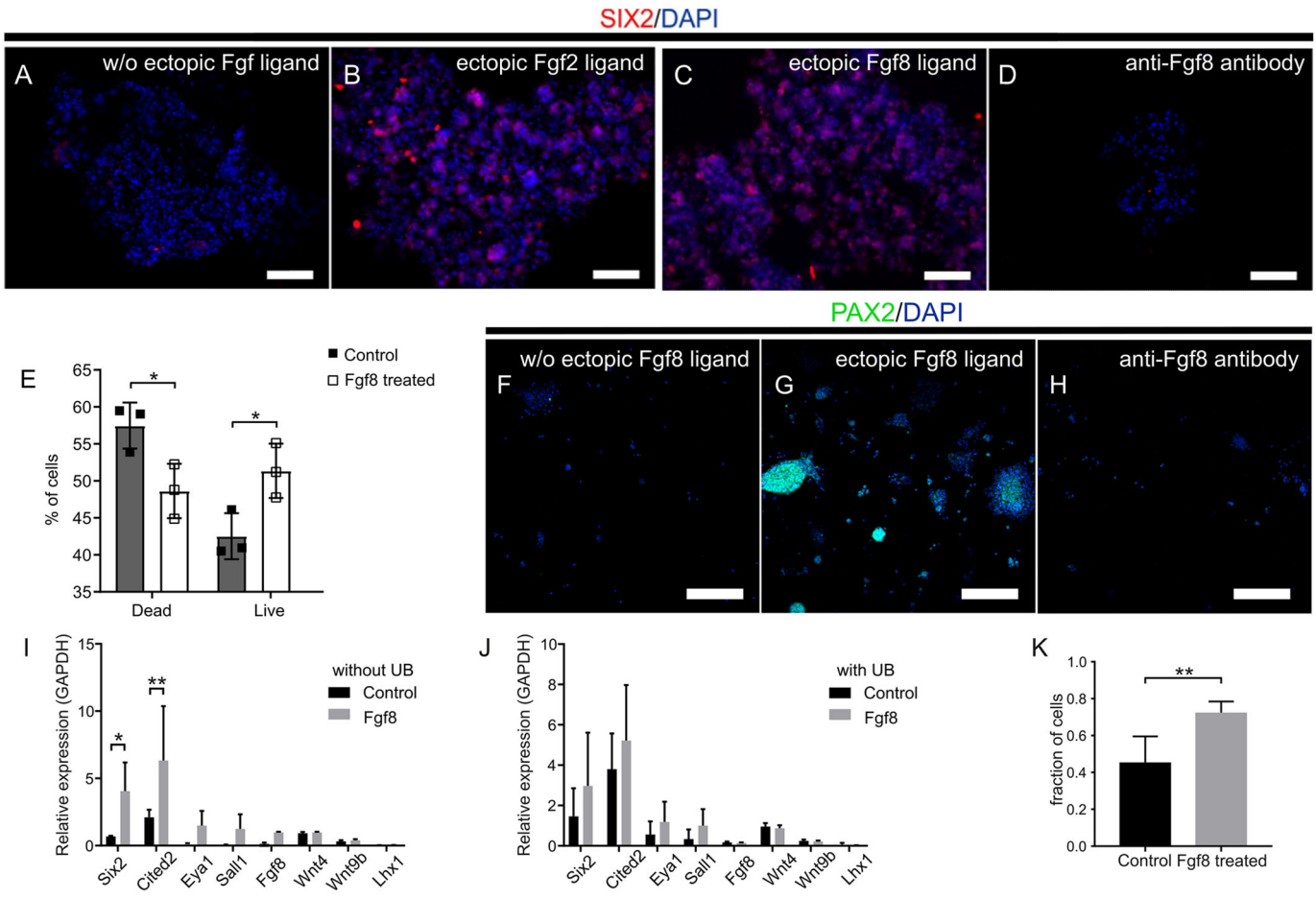

Fig. 3. Gene expression analysis in NPCs in the presence or absence of FGF ligand in nephrosphere assays. (A-D) Antibody staining of SIX2 expression with DAPI counterstaining. Scale bars: 100 µm. (A) NPCs lose the expression of SIX2 when the ectopic FGF ligand is not provided. (B,C) NPCs aggregate and retain SIX2 expression in the presence of ectopic FGF2 (B) or FGF8 (C) protein. (D) Loss of SIX2 expression in the presence of the anti-FGF8b antibody. (E) Loss of SIX2 expression and cell death in cultured nephrosphere assays treated with or without ectopic FGF8 ligand analysed by flow cytometry. Live and dead analysis was performed using flow cytometry (propidium iodide staining). P=0.0259 (dead) and P=0.0251 (live) (two-way ANOVA Sidak multiple comparisons; n=3). (F-H) Antibody staining for PAX2 expression counterstained with DAPI in cultured nephrospheres in the presence or absence of FGF8 ligand or in the presence of FGF8 antibody. Scale bars: 50 µm. (I,J) qPCR of tNPC gene expression in FGF8-treated nephrospheres (I) and in the presence of the UB (J). *P<0.05, **P<0.001 (two-way ANOVA Sidak multiple comparison; n=3). (K) Fraction of *Six2*$^{+}$ cells in response to ectopic Fgf8. Quantitative flow cytometry of dissociated E11.5 kidneys. Samples were collected using FACSCalibur and analysed using FlowJo. **P<0.001 (unpaired t-test; n=10).

UB outgrowth starts at around E10.5 when the metanephric mesenchyme is in a diffuse thickened state, inducing the patterning of the MM (Davies, 2016; Carroll et al., 2005; Perantoni et al., 1995; Mugford et al., 2008; Xu et al., 2014; Munro et al., 2017). At around E11, diffuse weak expression of *Fgf8* by MM cells coincides with the emergence of a well-defined cap mesenchyme (Davies, 2016; Carroll et al., 2005; Munro et al., 2017). Close to the UB, MM cells are rather immotile (Combes et al., 2016). Interestingly, sonic hedgehog (SHH), a repressor of *Fgf8* expression, is secreted from UB cells during early nephrogenesis (Yu et al., 2009; Lin et al., 2001). The SHH gradient emanating from the UB likely results in the lower *Fgf8* expression that is observed closer to the UB (Chen et al., 2016). A gradient of autocrine FGF8 signalling and thus chemokinesis would be in agreement with the previous observation that cell speeds increase with distance from the UB (Combes et al., 2016). In the same study, it was found that MM cells experience a subtle attraction towards the UB, indicating the presence of a UB-secreted chemotactic factor. WNT11 represents a likely candidate, as it is secreted already around E10.5-E11 by UB tip cells and is required for stable NPC-UB attachment (Carroll et al., 2005; O'Brien et al., 2018; Kispert et al., 1996; Uchiyama et al., 2010).

To analyse the interplay of chemical signalling and cell motility during mesenchymal condensation, we asked whether a model consisting of (1) FGF8-induced mesenchymal cell motility, (2) WNT11based chemoattraction and (3) SHH-induced repression of FGF8 close to the UB can explain mesenchymal condensation around the UB (Fig. 5A). In the computational model, NPCs are initially randomly positioned in a niche bordering a flat patch of the ureteric epithelium (Fig. 5E). The NPCs are assigned velocities that depend on the local FGF8 concentration, while the direction of movement is chosen randomly (Fig. 5A,B). Epithelial cells are secreting weak concentrations of both WNT11 and SHH, while scenarios of different levels of *Fgf8* expression by MM cells are explored (Fig. 5F,G; Fig. S3). Mechanically, all cells can adhere to each other when being closer than a threshold distance and detach when moving apart. Simulating this model results in an effective

Development (2022) 149, dev201012. doi:10.1242/dev.201012

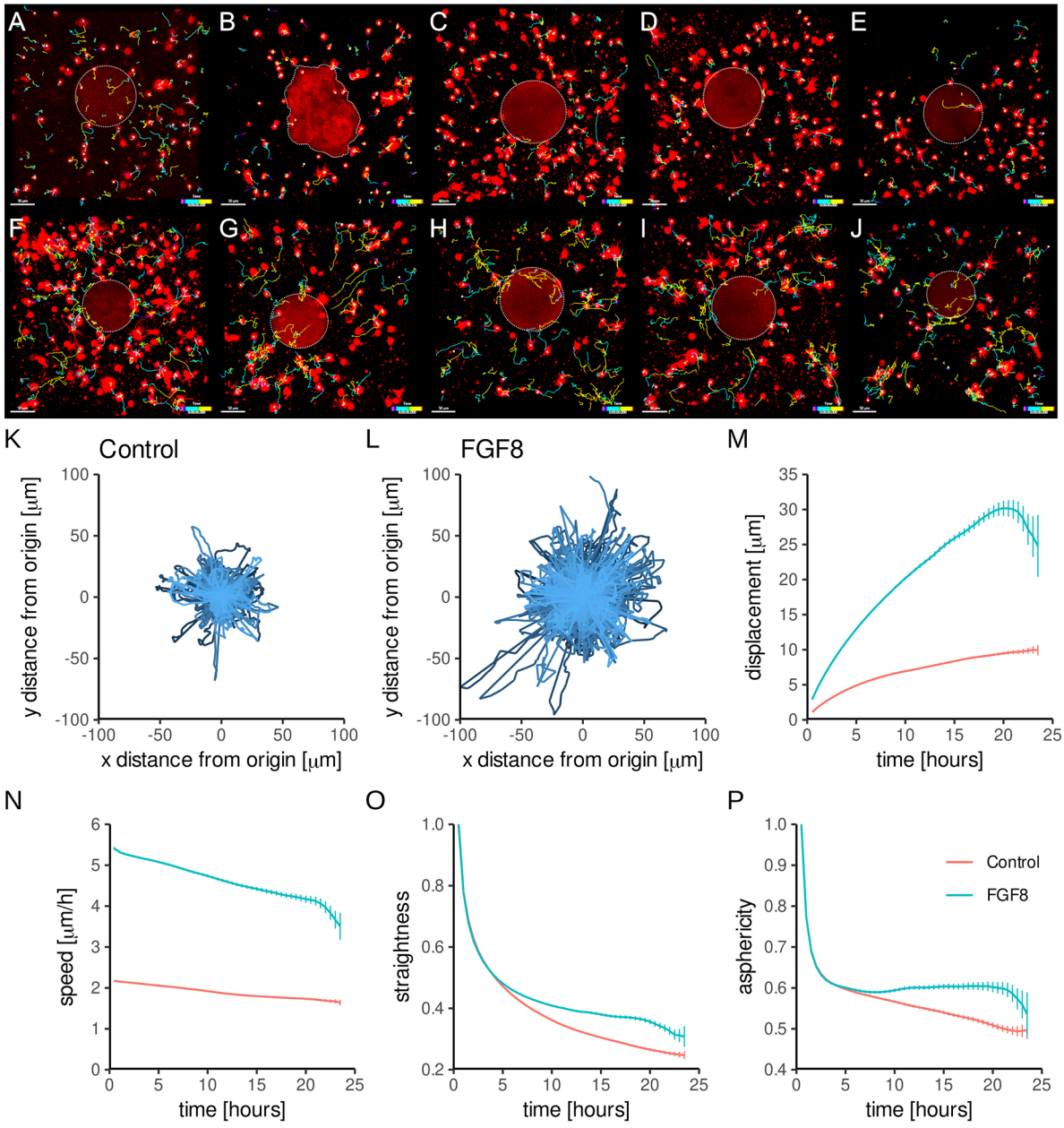

Fig. 4. Elevated and undirected NPC motility in response to FGF8. *In vitro* experiments with control beads (A-E) versus FGF8-soaked beads (F-J) in a culture of E11.5 MM cells (five samples each). Full cell tracks are shown after 24-h time lapse (FGF8, 534 tracks *in toto*; control, 538 tracks *in toto*). Cells were tracked for 24 h. Beads are outlined with dotted white lines. Scale bars: 50 µm. Tracks from all samples of each of the two cohorts were pooled (FGF8, 534 tracks; control, 538 tracks). Star plots of control (K) and FGF8 (L) experiments were normalized such that the start point of each track was at the origin. (M,N) Average displacement (Euclidean distance between track start and endpoints) and average speed over time. (O,P) Track straightness: displacement divided by contour length. Asphericity: the less spherically the steps of a track are distributed, the straighter the track (compare K and L with Mokhtari et al., 2013).

motility gradient with a trap-like region close to the epithelium (Fig. 5C,D,F; Fig. S3). At weak concentrations of FGF8, WNT11 and SHH, only the MM cells closest to the ureteric epithelium show strong displacement towards the ureteric epithelium, but most cells that are further away remain within a few cell diameters of their initial positions (Fig. 5C,F; Movie 3). At intermediate concentrations of FGF8 (twofold increase), most cells aggregate close to the basal surface of the ureteric epithelium (Fig. 5C,D,G). At higher FGF8 concentrations (threefold increase), cells aggregate everywhere in the niche, which is in line with our bead experiments (Fig. 5C; Movie 2, Movie 3). Last, we also observe FGF8 concentration peaks at locations where cells aggregate, resulting in swarm-like motility (Movie 3).

We conclude from these simulation results that the chemokinetic effect of FGF8 enables the niche-wide distribution of NPCs. This allows them to reach the vicinity of the UB and also to enter the sphere of influence of epithelial factors that support the immobilization of NPCs. The corresponding motility gradient that appeared in the simulations (Fig. S3) is in agreement with experimental observations (Combes et al., 2016). The simulations also show that excess FGF8 can override the guidance of epithelial signalling and prevent mesenchymal condensation.

Development (2022) 149, dev201012. doi:10.1242/dev.201012

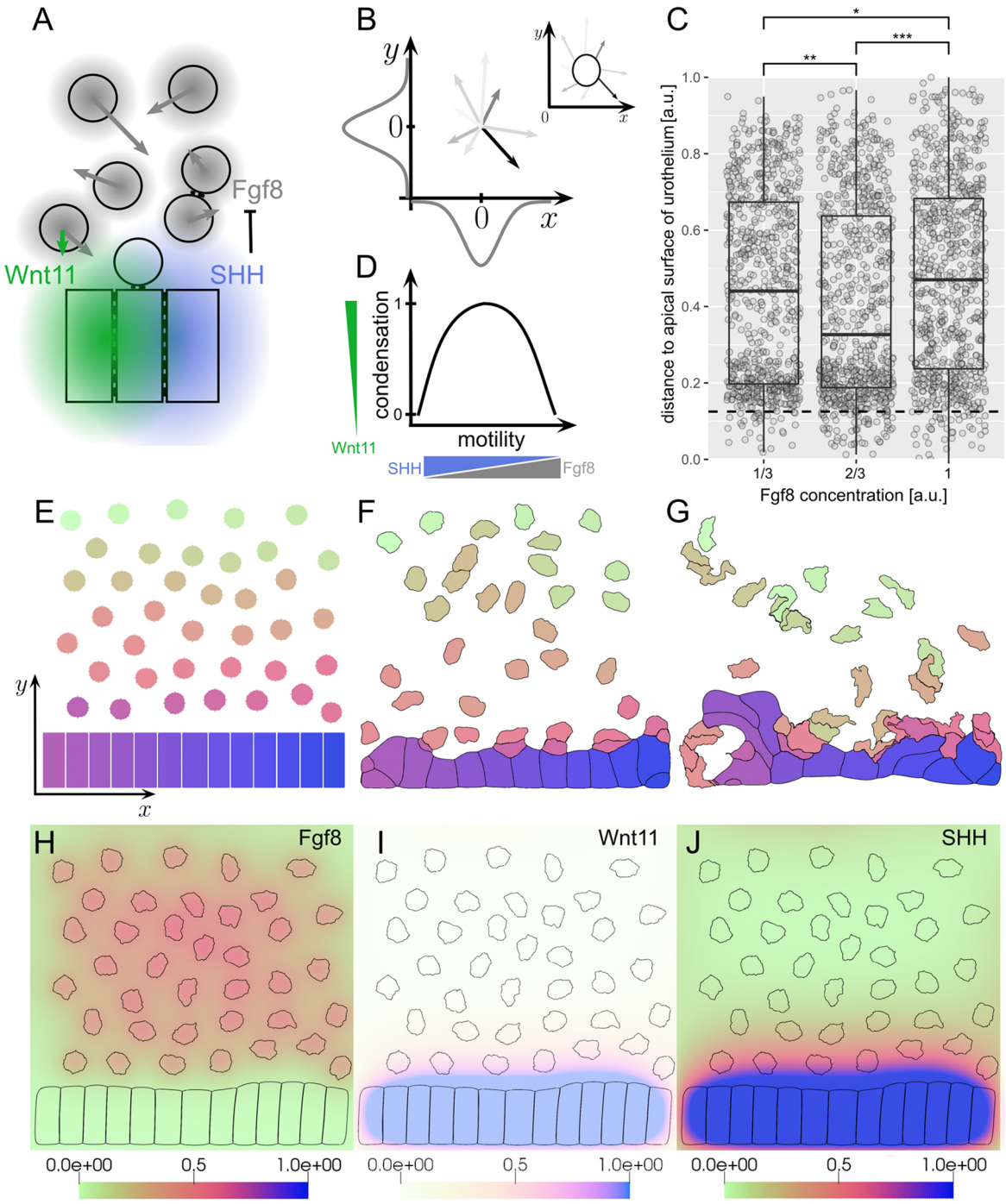

Fig. 5. 2D simulations of NPC condensation to the ureteric epithelium. (A) The simulation setup. NPCs express FGF8, can adhere to each other and the ureteric epithelium, and move with random velocities (the magnitude of which depends on FGF8 concentration). Ureteric epithelial cells also adhere to each other and secrete SHH, which represses *Fgf8* expression, and WNT11, which induces a weak attraction towards the ureteric epithelium (with one order of magnitude lower NPC speeds than with FGF8). NPCs close to the ureteric epithelium are immobilized due to SHH-induced repression of *Fgf8*. (B) Implementation of random cell motility. The components of the two-dimensional velocity vector for each cell GeometryNode are picked from normal distributions. Inset: example cell with velocities for a few GeometryNodes. In the simulations, each cell possesses several hundred GeometryNodes (see Materials and Methods). (C) Distance of NPCs to ureteric epithelium for simulations with an increasing FGF8 concentration. Only intermediate levels of FGF8 lead to more NPCs being trapped in the region close to the basal surface of the ureteric epithelium (dashed line). Data were pooled from n=20 simulations for each group. *P<0.1, **P<0.01, ***P<0.001 (Wilcoxon test). (D) Motility decreases with an increasing concentrations of SHH and increases with increasing concentrations of FGF8 and WNT11. Cells quickly condense with increasing FGF8 concentrations, reaching a maximum at intermediate FGF8 concentrations. At further increased FGF8 concentrations, NPC velocities are too elevated to be immobilized at the UB. WNT11 concentrations are one order of magnitude smaller than FGF8 concentrations and, accordingly, cell speeds (Table S4, Fig. S3). (E) Start configuration with dispersed NPCs over a flat patch of the ureteric epithelium. Colours correspond to cell identity. (F) Example of a final configuration with low FGF8 concentrations and limited NPC displacement. (G) Example of a final configuration with intermediate FGF8 concentrations, increased NPC displacement, mixing and strong condensation to the UB. (H-J) Examples of initial concentration gradients of FGF8, WNT11 and SHH. Colour codes represent normalized concentrations.

Development (2022) 149, dev201012. doi:10.1242/dev.201012

Deletion of *Fgf8* in late nephrons leads to hypomorph kidney phenotype

Deletion of *Fgf8* before gastrulation is lethal as cells lose the ability to migrate away from the primitive streak (Perantoni et al., 2005; Sun et al., 1999). Deletion of *Fgf8* in the MM using *Pax3*^{Cre} mice leads to the same phenotype, and new-born mice die shortly after birth (Grieshammer et al., 2005). We wondered whether FGF8 also plays a role in later stages of kidney development. *In situ* hybridization of *Fgf8* revealed its expression in upper cells forming PTAs and this expression was still maintained in the top cells of renal vesicles that form the future comma and S-shape bodies in wild-type kidneys (Fig. 6A-E). To investigate its effect during early nephron formation at PTA stage, we used later expression tissue-specific Cre mouse lines (see Materials and Methods). Cre was under the promoter of *Wnt4* or *Pax8* genes. By using this strategy, we generated mutant *Fgf8*$^{n/c}$ progeny with 50% frequency, while *Fgf8*$^{n/+}$ mice were used as littermate controls. First, to be sure that *Fgf8* did not have any function in the UB, we first deleted *Fgf8* from the UB using *HoxB7*^{Cre} mice; as expected, the mutant had no phenotype and the kidneys were similar to those of the wild-type mice (Figs S4C and S5A-D).

Second, we deleted *Fgf8* from MM cells by employing two tissue-specific Cre recombinase mice (under the promoter of *Pax8* and *Wnt4* genes). *Pax8*^{Cre} is expressed in both the MM and the UB tip (GUDMAP; Fig. S4A) (Bouchard et al., 2002; Harding et al., 2011), and *Wnt4*^{Cre} is expressed only in the MM (Fig. S4B; Shan et al., 2010). We found that the *Fgf8* deletion from the MM using either *Pax8*^{Cre} or *Wnt4*^{Cre} led to smaller kidneys when compared with littermate controls (Fig. 7A-C). On closer inspection, we found that in both cases kidneys had fewer mature nephrons when compared with littermate controls. Kidneys of *Fgf8*; (*Pax8*^{Cre}) revealed an arrest in S-shaped-body structures whereas the *Fgf8*; (*Wnt4*^{Cre}) showed comma-shaped body structures (Fig. 7D-I, higher magnification). Because the complete loss of FGF8 function during kidney development results in a failure of nephron formation around the S-shaped body stage (Perantoni et al., 2005; Grieshammer et al., 2005), these results raised the issue of whether there is still some *Fgf8* expressed in the *Fgf8*$^{n/c}$;*Pax8*^{Cre} and *Fgf8*$^{n/c}$;*Wnt4*^{Cre} kidneys. Therefore, we analysed the *Fgf8* expression in *Fgf8*$^{n/c}$;*Pax8*^{Cre} kidneys. Functional *Fgf8* RNA is expressed at a lower level than in the control litter analysed by qPCR, suggesting that the remaining *Fgf8* expression causes a hypomorph kidney phenotype. We observed levels of *Fgf8* expression that were around 40% of controls in E12.5 kidneys lacking *Fgf8* (Fig. 7J). These data demonstrate that FGF8 is required within the developing kidney to support the further development of the nephrons, and the reduced *Fgf8* expression during nephrogenesis induces hypomorph phenotypes.

Late deletion of *Fgf8* leads to incorrect localization of NPCs in the nephrogenic niche

tNPCs in the tip region of the UB are marked by *Six2* expression along with *Cited1*, *Cited2* and *Eya1* (Fig. 1) (O'Brien, 2019; Mugford et al., 2009; Brown et al., 2015; Tanigawa et al., 2016). *Wnt9b* that is expressed and secreted by the UB regulates the transition from tNPCs to cNPCs (Fig. 1) (Carroll et al., 2005). This transition is marked by a decrease of *Cited1* and *Cited2* expression (O'Brien, 2019; Brown et al., 2013; Mugford et al., 2009). At the same time, the expression of *Wnt4* in an aggregated subset of cNPCs that are located at the tip-trunk interface of the UB indicates the onset of nephron formation (Fig. 1) (Lawlor et al., 2019; Stark et al., 1994). When we compared the expression of *Six2* in wild-type kidneys with tissue-specific deletions of *Fgf8* in *Fgf8*$^{n/c}$;*Pax8*^{Cre} (MM and UB tip) or *Fgf8*$^{n/c}$;*Wnt4*^{Cre} (MM only) kidneys, we found an untypical *Six2*$^{+}$ expression patterns, indicating disorganized NPCs (Fig. 8A-C). Deletion of *Fgf8* in *Fgf8*$^{n/c}$;*Pax8*^{Cre} kidneys did not seem to alter the expression of *Wnt9b* when compared with the littermate controls (Fig. 8D-F) and, as expected, *Wnt9b* was not affected in *Fgf8*$^{n/c}$;*Wnt4*^{Cre} kidneys. On the other hand, the expression of *Wnt4* was decreased in both *Fgf8*$^{n/c}$;*Pax8*^{Cre} and *Fgf8*$^{n/c}$;*Wnt4*^{Cre} kidneys (Fig. 8H,I) as compared to the littermate controls (Fig. 8G). Further, in both *Fgf8*$^{n/c}$;*Pax8*^{Cre} and *Fgf8*$^{n/c}$;*Wnt4*^{Cre} kidneys, condensation of NPCs expressing *Eya1* and *Six2* around the UB was perturbed, while the expression of *Cited1* was still maintained in the *Fgf8*$^{n/c}$;*Wnt4*^{Cre} kidneys but not in the *Fgf8*$^{n/c}$;*Pax8*^{Cre} kidneys (Fig. 8K,L,N,O). Together, these data show that these anchor genes for the NPC compartment have an incorrect pattern where *Fgf8* is deleted via either *Pax8*^{Cre} or *Wnt4*^{Cre} mouse lines.

Without the expression of *Fgf8* after kidney induction, NPCs still accumulate at the tip of the UB

To further confirm the results obtained from our *in vitro* experiments (cultured *Fgf8*$^{n/c}$;*T*^{Cre} kidneys and the effect of FGF8 on MM cells in the bead culture experiment), we stained NPCs and UB cells using fluorescent markers on *Fgf8*$^{n/c}$;*Pax8*^{Cre} and *Fgf8*$^{n/c}$;*Wnt4*^{Cre} mice that delete *Fgf8* later in nephrogenesis (after E11.5). To analyse the complete PTA formation, we have selected the E16.5

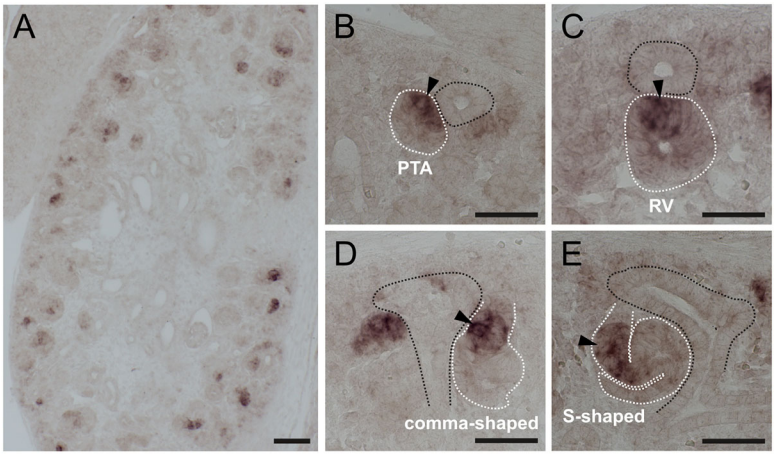

Fig. 6. *In situ* hybridization of FGF8 in E15.5 embryonic mouse kidney. Taking a closer look at MM derivatives (B-E), the expression of FGF8 is localized closer to the UB tip. (A) 10× magnification of E15.5 kidney. (B-E) 43× magnified selections. Dotted black lines indicate the ureteric epithelium; dotted white lines indicate (B) pretubular aggregate (PTA), (C) renal vesicle (RV), (D) comma-shaped body and (E) S-shaped body. Black arrowheads indicate cells expressing Fgf8. Scale bars: 100 µm in A; 50 µm in B-E.

Development (2022) 149, dev201012. doi:10.1242/dev.201012

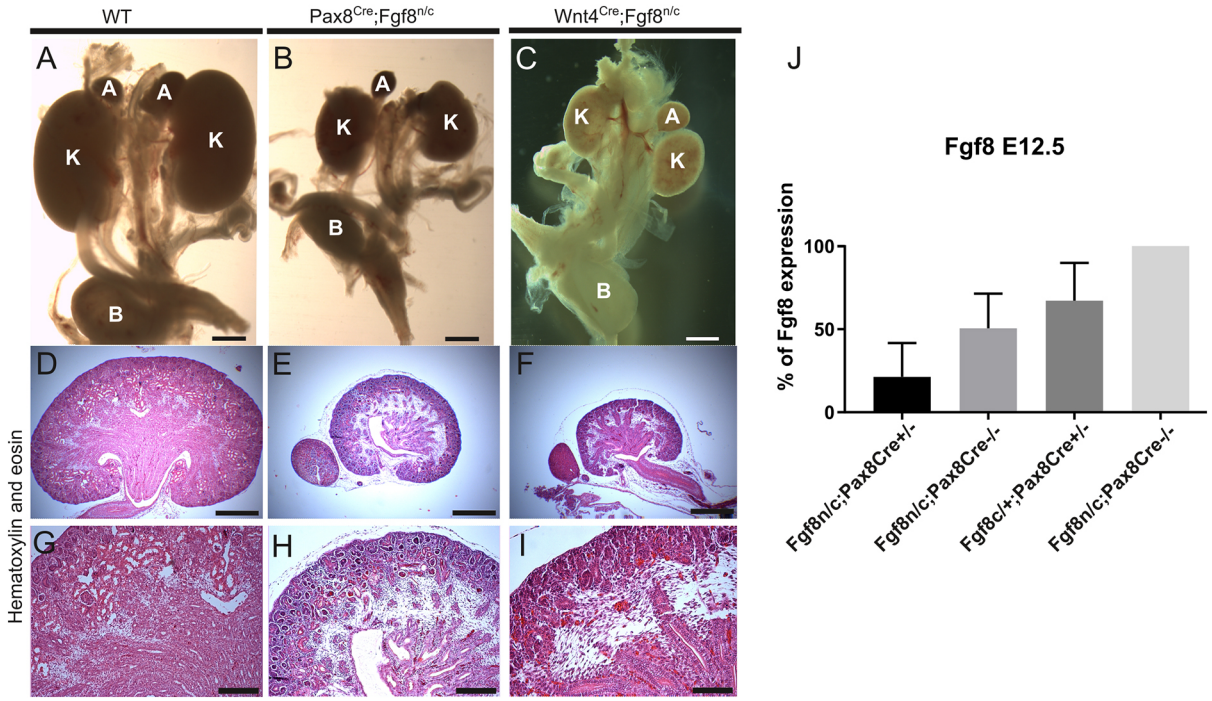

Fig. 7. *Fgf8* deletion in E16.5 hypomorph mouse embryos. (A-C) The deletion of *Fgf8* from the metanephric mesenchyme led to smaller kidneys when compared with littermate controls. (A) Urogenital system of littermate controls, (B) Cre-mediated deletion of *Fgf8* using *Pax8*^{Cre} and (C) *Wnt4*^{Cre}. (E,F,H,I) Hematoxylin and Eosin staining shows smaller kidneys lacking mature nephrons when compared with controls (D,G). (G-I) Higher magnifications than D-F. (J) qPCR of *Fgf8* in E12.5 kidneys of *Fgf8 Pax8*^{Cre}. A, adrenal gland; K, kidney; B, bladder. Scale bars: 500 µm for A-F; 100 µm for G-I.

stage where most of the PTAs are already formed. Staining of *Six2*$^{+}$ NPCs in E16.5 kidneys obtained from crossing *Fgf8*$^{n/c}$ and *Pax8*^{Cre} revealed a thicker cap mesenchyme at the tips of UBs, suggesting differences in niche composition when compared with littermate controls (Fig. 9A,B). A thicker layer of *Six2*$^{+}$ cells in the tip region of the UB indicates that NPCs either failed to fully condense around the UB or that they were not primed as cNPCs (Fig. 9C). Similar results were obtained when *Fgf8* was deleted using *Wnt4*^{Cre} (Fig. 9D,E). With *Wnt4*^{Cre}-mediated deletion of *Fgf8*, the *Six2*$^{+}$ population failed to condense around the UB tip, as seen after

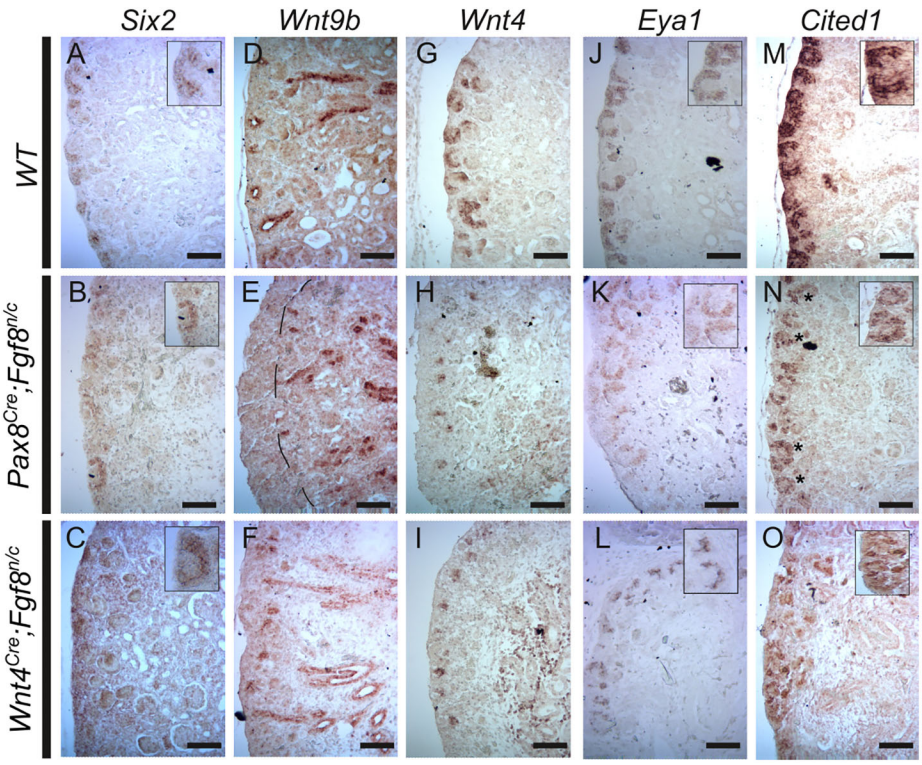

Fig. 8. Gene expression in littermate control and hypomorph mutant kidneys by *in situ* hybridization. (A-C) Expression of *Six2* was observed around UB tips on the kidney cortex, but in mutant kidneys underexpressing *Pax8* or *Wnt4* Cre its expression was disorganized. (D-F) Expression of *Wnt9b* was restricted to the UB in littermate controls; *Pax8*^{Cre}- and *Wnt4*^{Cre}-mediated *Fgf8* deletion. (G-I) *Wnt4* expression was observed in littermate controls and mutants, but the expression was reduced in the mutant kidneys. (J-O) Expression of *Eya1* (J-L) and *Cited1* (M-O) was also disorganized in mutant kidneys when compared with littermate controls. Higher magnification of the staining to visualize the disorganization of the expressing cells is shown in the insets. Scale bars: 100 µm.

Development (2022) 149, dev201012. doi:10.1242/dev.201012

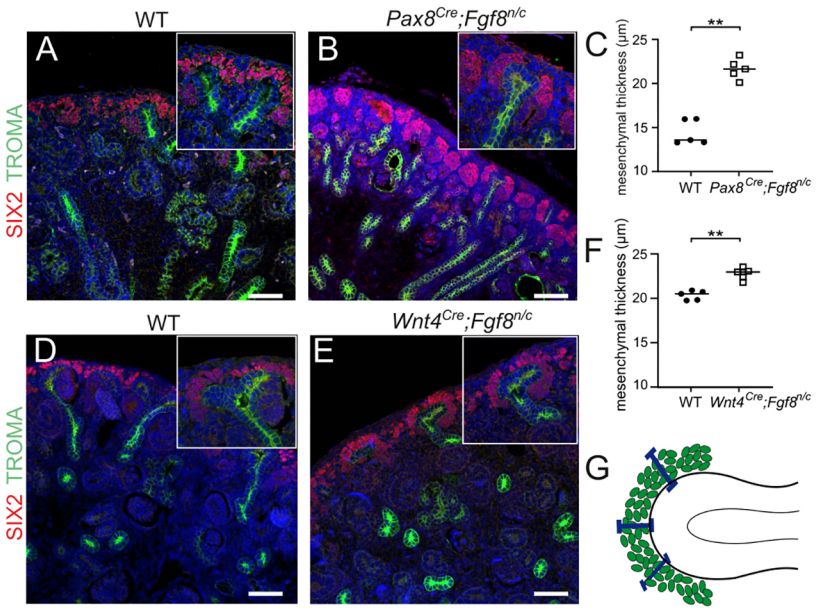

Fig. 9. Accumulation of NPCs in the tip region in hypomorph kidneys. (A,B,D,E) When *Fgf8* was deleted using *Pax8*^{Cre} (B) or *Wnt4*^{Cre} (E), NPCs did not form a condensed cap mesenchyme, but they rather accumulated at the tip region of the UB when compared with the littermate controls (A,D). The insets are higher magnifications. (C) Distance of the last layer of the NPCs from the UB tip of E16.5 *Fgf8*$^{n/c}$;*Pax8*^{Cre} kidneys. (F) Distance of the last layer of the NPCs from UB tip of E16.5 *Fgf8*$^{n/c}$;*Wnt4*^{Cre} kidneys. (G) How the measurements were made for calculating the distance of NPCs around the UB tip. Kidneys were stained for SIX2 (NPCs, red) and TROMA (UB, green), and DNA was counterstained using Hoechst 33342 (blue). $^{**}P<0.01$ (unpaired *t*-test; $n=6$). Scale bars: 100 µm.

Pax8^{Cre}-mediated deletion of *Fgf8* (Fig. 9F). LIM-class homeodomain transcription factor 1 (LHX1) is a known crucial marker for nephron patterning and maturation (Kobayashi et al., 2005; Liu et al., 2018). In E16.5 wild-type and *Fgf8*$^{n/c}$;*Wnt4*^{Cre} kidneys, LHX1 stained RV, CB and SB structures, whereas in *Fgf8*$^{n/c}$;*Pax8*^{Cre} kidneys the expression was only found in RV and CB, demonstrating that nephron maturation is delayed (Fig. S6A-D). These results confirm the observations from the *in situ* hybridization experiments (Fig. 8), suggesting that the *Six2*$^{+}$ NPCs accumulate around the UB tip and that NPC induction is impeded, inducing a delay of nephron development.

DISCUSSION

Intercellular signalling between NPCs and UB cells is key for mammalian kidney development, and it is known to be tightly controlled. Failure of the expression of key genes such as *Six2*, *Fgf8*, *Wnt4*, *Wnt9b* and others leads to developmental defects or even to embryonic lethality (O'Brien, 2019; Oxburgh, 2018; Stark et al., 1994; Perantoni et al., 2005; Grieshammer et al., 2005). FGF8 is also known to be involved in the activation of the kidney-specific genes *Wnt4* and *Lim1* (*Lhx1*) (Perantoni et al., 2005; Huh et al., 2020).

In this work, we have used several cre-based mouse lines to establish that *Fgf8* expression is located in the MM and imparts its function on the nephron progenitor cells. Deletion of *Fgf8* from the MM resulted in embryonic kidneys that lacked mature nephrons, which led to smaller hypomorphic kidneys and postnatal death. As *Fgf8*-deficient kidneys lack *Wnt4* expression, *Fgf8* is required for *Wnt4* expression (Perantoni et al., 2005; Grieshammer et al., 2005). Although it is known that WNT4 initiates MET (Stark et al., 1994), in accordance with previously published results, we also observed that, independently of WNT4, FGF8 is required for the condensation of NPCs (Perantoni et al., 2005). We found that in kidneys where FGF8 signalling was blocked using an anti-FGF8 antibody, NPCs did not condense to form pretubular aggregates. But upon removal of the antagonizing agent, PTA formation was recovered. This indicates that, even though FGF8 is upstream of WNT4, it regulates NPC condensation, which is itself required for PTA formation before WNT4-induced MET of PTAs.

FGFs are also involved in the maintenance of NPCs during early nephrogenesis (Brown et al., 2011). Although previously only a modest effect of FGF8 on cap marker transcription was observed in 2D cultures (Brown et al., 2011), our results with 3D cultures show that without FGF8, *Six2* expression is lost, but when ectopic FGF8 is added and in the presence of the UB, the expression of *Six2* is maintained when compared with the vehicular control. Similarly, the expression of other tNPC markers, such as *Cited1*, *Cited2* and *Eya1* is also maintained in the presence of FGF8. We explain the discrepancy with the previous observations through improved culture conditions, as it has been shown that culturing NPCs in a 3D micro-environment leads to an improvement in nephrogenic potential (Li et al., 2016). In conclusion, FGF8 seems to be required for the expression of tNPC markers and thus tNPC maintenance, although it might not determine NPC fate, as cNPCs that form PTAs also express FGF8.

To understand how FGF8 might contribute to the formation of the cap mesenchyme, we used a computational model combining FGF8-induced chemokinesis with weak repressive and attractive chemical signals released from the epithelium. Our simulations showed that this results in graded motility perpendicular to the UB surface and thus a trap-like region near the UB that immobilizes passing NPCs. In our model, the specific balance between FGF8-induced NPC motility and epithelial signalling is evident. How this balance is achieved, whether through the precise control of morphogen gradients or based on heterotypic interactions between NPCs and UB cells, remains to be elucidated.

Our results suggest that FGF8 is an autocrine chemokinetic factor expressed in the metanephric mesenchyme and is required for the condensation of NPCs while being involved in the maintenance of tNPCs. It is known that the FGF8 ligand interacts with several FGF receptors and that this interaction can also be modulated by heparan sulphate proteoglycans, which consequently affect the spatio-temporal gradient of FGF8 concentration (Krishnan Harish et al., 2022 preprint). Yet self-organized motility, such as we observed in the NPCs with FGF8, may provide adaptability to changes in the microenvironment. To fully understand how FGF8 mediates its function, a detailed elucidation of the ligand-receptor interaction *in vivo* is required.

Development (2022) 149, dev201012. doi:10.1242/dev.201012

MATERIALS AND METHODS

Mouse strains and tissue collection

In this work, the mouse experiments were conducted in accordance with the Finnish and EU legislation. The Finnish National Animal Experiment Board approved all animal experiments, and experiments were conducted under internal licences issued by the Laboratory Animal Centre of the University of Oulu, Finland. To delete *Fgf8* from mouse kidneys, we crossed $Fgf8^{\Delta 2,3/+}$ males with $Pax8^{Cre/+}$ female. The progeny were genotyped and females with a $Pax8^{Cre/+}$;$Fgf8^{n/+}$ genotype were crossed with $Fgf8^{Floxed/Floxed}$ males. The progeny were genotyped and embryos with the genotype $Fgf8^{n/c}$;$Pax8^{Cre/+}$ were selected for the experiments. A similar strategy was used for $Wnt4^{eGFPCre/+}$ and $HoxB7^{Cre/+}$. To delete *Fgf8* using T^{Cre}, a similar strategy was employed to that of Perantoni et al. (2005). Briefly, females with genotype $Fgf8^{Floxed/Floxed}$ were crossed with males with genotype $T^{Cre/Cre}$;$Fgf8^{\Delta 2,3/+}$ and progeny with a genotype of $T^{Cre/+}$;$Fgf8^{n/c}$ were used for this study. Expression of *Cre* and deletion of *Fgf8* were assessed by genomic PCR, as described by Perantoni et al. (2005). Timed matings were checked at noon for the presence of a vaginal plug, which was considered to be E0.5 when identified. To obtain unbiased kidney samples, male and female embryos were collected from pregnant females that were euthanized with CO_2 followed by cervical dislocation, as per the institutional guidelines. Embryos were collected in sterile PBS and kidneys were dissected in 1×PBS with calcium and magnesium. Dissected kidneys were further treated depending on the experiment. Details of the mouse lines used in this work can be found in Table S1.

Histology and immunofluorescence

Hematoxylin and Eosin staining

For light microscopy, paraffin wax-embedded kidney sections were stained with Hematoxylin and Eosin, following standard procedures according to Veikkolainen et al. (2012).

Immunostaining

Embryonic kidneys were collected and dissected at E11.5, E12.5, E16.5 and P0 from genotyped mutant and littermate controls. Samples were fixed in 4% paraformaldehyde (PFA) overnight at 4°C and dehydrated in serial dilutions with 25% ethanol→50% ethanol→75% ethanol→100% ethanol in water with an incubating time in each step of 45 min or until the sample sank to the bottom of the test tube. At this point, the samples were transferred to a clearing solution (xylene), twice, for 60 min each. Samples were moved to melted paraffin wax, thrice, for 60 min each, and then these samples were carefully embedded in paraffin wax blocks and stored at 4°C. Embedded samples were sectioned (14 µm) with Lecia microtome, and slides were prepared with up to four samples on each slide. To perform staining, sections were selected and slides were prepared by heating at 55°C to melt the paraffin wax. To deparaffinize, slides were incubated in xylene solution, twice, for 5 min each. To remove xylene, slides were incubated in the 100% ethanol, twice, for 5 min each, and then hydrated in 95% ethanol→75% ethanol→50% ethanol in water for 5 min each. Antigen retrieval was performed in 1 mM EDTA-NaOH solution (pH 8.0) or 10 mM sodium citrate-citric acid solution (pH 6.0) in pressure cooker for 10 min (Pileri et al., 1997). After antigen retrieval, samples were incubated, for 60 min, in blocking solution [1×PBS+0.01% Triton-X100+serum (serum was selected based on antibody reactivity)]. Incubation duration and temperature were tested for each primary antibody and used accordingly. Images were acquired on an Olympus BX51WI upright microscope with Hamamatsu ORCA-ER digital camera.

Nephrospheres

A sphere-forming assay was performed as described previously with minor modifications (Ihermann-Hella et al., 2018). MMs from E11.5 kidneys from CD-1 mice were dissociated with TripLE Express (Gibco) or with a mix of collagenase type 3 (Worthington Biochemical, LS004180) and DNase I (New England Biolabs, M0303S) for 5 min in 37°C in Hepes buffer (pH 7.35) at 37°C for 15 min. To obtain a single-cell suspension, after stopping the activity of the enzymes with complete media, the cell suspension was strained through 0.45 µm cell strainer. The total obtained cell suspension was divided into four equal parts, from which each part was mixed with two parts of Matrigel (Corning, 354277) and allowed to attach for 10 min at 37°C, 5% CO_2 and 95% humidity. Media containing a Src-kinase inhibitor (10 µM PP2; Tocris Bioscience, 1407) and/or FGF8b (100 ng/ml; R&D Systems, 423-F8) 24 h was added to the polymerized mix cells and Matrigel.

Real-time qPCR

To remove nephrospheres from the embedded Matrigel, plates were chilled on ice for 1 h on a shaking platform. Liquefied Matrigel solution was collected and centrifuged at 10,621 ***g*** at 4°C for 10 min. The pellet was washed twice with DEPC-treated 1×PBS at 2655 ***g*** at 4°C for 5 min and flash-frozen in liquid nitrogen until required. RNA extraction was performed using RNeasy mini (Qiagen, 74104) and cDNA synthesis was performed using the First Strand cDNA synthesis kit (Thermo Fisher Scientific, K1612), where 100 ng of RNA was used as a template. cDNA was diluted 1:1 with PCR grade water; for the qPCR reaction, 2 µl cDNA was mixed with 1.2 µl each of forward and reverse primer (Table S3) along with 0.6 µl of PCR water and 5 µl Brilliant Sybr Green III qPCR master mix (Agilent Technologies, 600882). qPCR was carried out at CFX96 Touch System (Bio-Rad) with a program of 95°C for 10 min, 40 cycles of 95°C for 20 s, 60°C for 20 s and 72°C for 20 s, followed by a melt curve. qPCR was performed with three biological replicates in three technical replicates.

Western blotting and antibody validation

For the validation of anti-FGF8b antibody, a Flag-tagged FGF8b clone was obtained from Genscript CloneID: OMu22892D (NCBI Nucleotide: NM 001166361.1) and was overexpressed in CHO-K1 cells (ATCC, CCL-61). The media were collected from FBS-starved CHO-K1 cells expressing FGF8b and precipitated using the TCA method as described previously (Fic et al., 2010). Western blotting was carried out with controls (commercially bought rmFGF8b and cell lysate of validated protein-expressing Flag tag and CHO-K1 cell lysate).

For GSK3β quantification, a nephrosphere culture was established (see 'Nephrosphere' section). The cells were extracted as described in the section 'Real time qPCR'. Cells were lysed using 1×RIPA cell lysis solution (Cell Signaling, 9806) supplemented with cOmplete, Mini, EDTA-free Protease Inhibitor Cocktail (Roche, 04693159001). Protein quantity estimation was performed using the a BCA Protein Assay Kit (Pierce, 23225). 50 mg of total protein was loaded onto in-house prepared 12.5% SDS-PAGE separating gel and 6% stacking gel, and separation was performed for 90 min at 110 V at room temperature. Transfer was carried out onto NCP Porablot Membrane (Macherey-Nagel, 12807411) for 90 min at 90 V at 4°C. The membrane was blocked with 5% BSA solution and all the primary antibodies were incubated overnight at 4°C, while secondary antibodies were incubated for 60 min at room temperature (Table S2). The detection was performed using LumiGLO Reagent (Cell Signaling, 7003S) on a Fujifilm LAS-3000 Imager. For sequential protein detection, the antibodies were stripped away, by incubating the membranes with 0.2 M NaOH solution for 15 min at room temperature and re-blocking with BSA. The protein quantitation was performed using an ImageQuant TL8.1 (Cytiva LifeSciences).

In situ hybridization

The non-radioactive section *in situ* hybridization technique was performed as described previously (Junttila et al., 2015). The used cDNA probes *Wnt4*, *Wnt9b*, *Six2*, *Eya1* and *Cited1* were gifts from Prof. Thomas Carroll (University of Texas Southwestern Medical Center, Dallas, TX, USA).

Flow cytometry

Dissected E11.5 kidneys were cultured in a Trowell culture system. After 3 days of culture with or without rmFGF8b, kidneys were dissociated into a single-cell suspension. Cells were fixed with 4% PFA and permeabilized with cytofix/cytoperm (BD Biosciences, 554714) as per the manufacturer's instructions. Samples were stained using primary anti-SIX2 antibody (Table S2) for 30 min on ice, washed and then stained using secondary goat

Development (2022) 149, dev201012. doi:10.1242/dev.201012

anti-rabbit AlexaFluor 488 (Table S2) for 30 min on ice and washed thoroughly. Samples were scored on a FACSCalibur (BD Biosciences). Three biological repeats were carried out for each condition while maintaining the protocol and template for sample acquisition.

Cap mesenchymal quantifications

Sections of E16.5 $Pax8^{Cre}$;$Fgf8^{n/c}$ and E11.5 T^{Cre};$Fgf8^{n/c}$ kidneys were cultured for 3 days in Trowell culture, fixed and stained using anti-SIX2 (Table S2) and anti-TROMA (Table S2) antibodies and counterstained with Hoechst 33342 (Thermo Fisher Scientific, H3570). Imaging was carried out with Zeiss LSM 780 confocal microscope and samples were analysed on a Zen Blue (2012 edition, Zeiss). The distance between the pair of $Six2^+$ cells closest and most distant to the UB was measured repeatedly along the UB at intervals of one cell length to determine the thickness of the cap mesenchyme. Additionally, the dispersion of NPCs was quantified as the Euclidean distance between NPCs and UB surfaces. Using Bitplane Imaris 9.6.0 and the Imaris modules Measurement Pro and Vantage, NPC positions were quantified using fluorescence intensity-based spot detection; UB surfaces were segmented using fluorescence intensity-based 3D segmentation. To determine the proportions of attached and free or unattached $Six2^+$ cells in both controls and mutant kidneys, cells were classified as attached when their centroid positions were closer to the UB than twice the median distance (17.4 µm) of all centroid positions of the $Six2^+$ cells in the control kidneys.

Bead assays with NPCs

A sphere-forming assay was modified to induce cell motility in response to FGF8. Metanephric mesenchyme cells were dissociated into a single-cell suspension and an equal amount of cells were divided and mixed with Matrigel. BSA-soaked or FGF8 (100 µg/µl) -soaked agarose blue beads (Affi-Gel Blue Gel, Bio-Rad, 1537302) were carefully placed in individual wells of a four-chamber 35 mm glass-bottom dish (Cellvis, D35C4-20-0-N). The Matrigel cell mixture was carefully applied to the surface of the beads and placed in a pre-equilibrated microscopic chamber maintained at 37°C and 5% CO_2. Time-lapse was performed with Leica SP8 falcon 20× water immersion lens for 24 h. Cells were tracked using the Imaris (v9.6; BitPlane) cell tracking functionality. Cell tracks from different samples (n=5 each) were pooled and analysed using the R package CelltrackR (Wortel et al., 2021).

Modelling

Parameter values for the simulation of mesenchymal condensation in the nephrogenic niche. One length unit of the simulation box corresponds to half a micron, i.e. $\Delta x = \frac{0.5\,\mu\text{m}}{1\text{ LB length}}$ and $2 \cdot 10^5$ iterations correspond to 12 h of developmental time, i.e. $\Delta t = \frac{12\text{ h}}{2 \cdot 10^5\text{ iterations}} = \frac{0.216\text{ s}}{\text{iteration}}$. The diffusion coefficient D of the morphogens is related to the LB relaxation time τ via $D = \frac{1}{3}\left(\tau - \frac{1}{2}\right) \cdot \frac{\Delta x^2}{\Delta t}$ (Tanaka et al., 2015). The gradient length $\lambda = \sqrt{D/d}$ of an exponential gradient $c(x)=c_0 e^{-x/\lambda}$ is the distance at which the concentration has decreased to $c(\lambda)=c_0/e$. $[\,]_{cell}$ is the median intracellular concentration. Mass source strength as well as production and degradation rates refer to the PhysicalNodes, which represent the discrete grid on which the fluid and the morphogens live (Tanaka et al., 2015). The area of an NPC or an epithelial cell comprises a few hundred PhysicalNodes; the simulation box comprises exactly $300 \cdot 300$ PhysicalNodes. Morphogen dynamics are described in the section 'Setup'. Our model uses a cell-based Lattice-Boltzmann Immersed-Boundary simulation framework for morphogenetic problems (Tanaka et al., 2015). Model parameter values are shown in Table S4.

Setup

We simulated mesenchymal condensation within a 150 µm^2 section of the nephrogenic niche containing randomly dispersed NPCs and a flat patch of ureteric epithelium for an interval of 12 h, corresponding to embryonic days E10.5 to E11 (Fig. 5D, Movie 3).

The model represents the dynamics of FGF8, SHH and WNT11 concentrations by the following differential equations:

$$\begin{aligned}\partial_t[FGF8] &= D\Delta[FGF8] + \rho_{FGF8}H^S - ([SHH]) - \delta_{FGF8}\\ \partial_t[SHH] &= D\Delta[SHH] + \rho_{SHH} - \delta_{SHH}\\ \partial_t[WNT11] &= D\Delta[WNT11] + \rho_{WNT11} - \delta_{WNT11}\end{aligned},$$

where ∂_t is the time derivative, D is the diffusion coefficient, Δ denotes the Laplacian operator, ρ and δ are the production and degradation rates, and H^{S-} is the shifted Hill function. Parameter values are shown in Table S4.

Measurements

At the end of each simulation, the distance of all NPC centroids to the centroid of the ureteric epithelium was measured. All data were pooled and visualized as a boxplot (Fig. 5C) using R (R Core Team., 2020). The significance level was determined based on a Wilcoxon signed-rank test and added to the boxplot.

Cells

Cells are represented by highly resolved 2D polygonal geometries with a cortical tension established by elastic forces between GeometryNodes (Tanaka et al., 2015). Similarly, cell adhesion is realized by elastic forces between neighbouring cells. GeometryNodes are added or removed when the distance between GeometryNodes, i.e. cell size, changes. Similarly, adhesions are created or removed based on a distance threshold between intercellular GeometryNodes. The cells are immersed in a Newtonian fluid and no-flux boundary conditions are imposed on the domain boundaries.

Morphogens

Morphogens are produced and degraded within cells, can freely diffuse within the entire domain and through cell boundaries, and are advected by motile cells. Parameter values are shown in Table S4.

Cell motility

Random motility is established by applying 2D velocities to each GeometryNode, where velocities are picked from a normal distribution whose standard deviation is proportional to the median local FGF8 concentration (Fig. 5B). Similarly, a weak attractive force is established by picking positive 1D velocities (directed towards the UB) from a uniform distribution where the upper bound is proportional to the median local WNT11 concentration.

Acknowledgements

We thank Ms Paula Haipus, Ms Johanna Kekolahti-Liias and Ms Hannele Härkman for excellent technical assistance, Prof. Maxime Bouchard for providing $Pax8^{Cre}$, $Fgf8^{Floxed/Floxed}$ and $Fgf8^{\Delta 2,3/+}$, and Prof. Andy McMahon for $Hoxb7^{Cre}$ mouse line. We also thank Tiina Jokela for collecting the mouse samples and establishing the protocol for genotyping. We thank Dr Alan O. Perantoni and Dr Mark B. Lewandoski for providing us with T^{Cre};$Fgf8^{n/c}$ mouse embryonic kidneys. Dr Veli-Pekka Ronkainen is acknowledged for helping us set up the time-lapse imaging and the Vainio lab for helpful discussions. M.M. thanks Harold Gomez for discussions on image analysis and Lisa Conrad for comments on the manuscript. Confocal imaging was conducted at the Light Microscopy Unit of Biocenter Oulu, University of Oulu. Imaging was performed at the Biocenter Oulu Light Microscopy Core Facility, University of Oulu, Finland, supported by Biocenter Finland.

Competing interests

The authors declare no competing or financial interests.

Author contributions

Conceptualization: F.N.; Methodology: A.S., M.M., A.D., A.I.-H., S.K.; Software: M.M., D.I.; Formal analysis: A.S., M.M., F.N.; Investigation: F.N.; Writing - original draft: A.S., M.M., F.N.; Writing - review & editing: A.S., M.M., A.D., A.I.-H., S.K., S.J.V., D.I., F.N.; Supervision: S.K., S.J.V., D.I., F.N.; Funding acquisition: S.J.V., D.I., F.N.

Funding

This work was funded by the Academy of Finland (206038, 121647, 250900, 251314 and 260056 to S.J.V.; 243014583 to F.N.), by Tekes BioRealHealth (24302443 to S.J.V.), by the Svenska Kulturfonden, by the Suomen Kulttuurirahasto (Pekka ja

Jukka-Pekka Lylykarin rahasto) and by the Schweizerischer Nationalfonds zur Förderung der Wissenschaftlichen Forschung (CRSII5 170930 to M.M. and D.I.).

Data availability

The computer modeling program ha been deposited in Gitlab (https://git.bsse.ethz.ch/iber/Publications/2022_Meer_NPC_Condensation)

Peer review history

The peer review history is available online at https://journals.biologists.com/dev/lookup/doi/10.1242/dev.201012.reviewer-comments.pdf

References

Bae, Y.-K., Trisnadi, N., Kadam, S. and Stathopoulos, A. (2012). The role of fgf signaling in guiding coordinate movement of cell groups: guidance cue and cell adhesion regulator? *Cell Adhes. Migr.* **6**, 397-403. doi:10.4161/cam.21103

Bouchard, M., Souabni, A., Mandler, M., Neubüser, A. and Busslinger, M. (2002). Nephric lineage specification by pax2 and pax8. *Genes Dev.* **16**, 2958-2970. doi:10.1101/gad.240102

Brown, A. C., Adams, D., de Caestecker, M., Yang, X., Friesel, R. and Oxburgh, L. (2011). Fgf/egf signaling regulates the renewal of early nephron progenitors during embryonic development. *Development* **138**, 5099-5112. doi:10.1242/dev.065995

Brown, A. C., Muthukrishnan, S. D., Guay, J. A., Adams, D. C., Schafer, D. A., Fetting, J. L. and Oxburgh, L. (2013). Role for compartmentalization in nephron progenitor differentiation. *Proc. Natl Acad. Sci. USA* **110**, 4640-4645. doi:10.1073/pnas.1213971110

Brown, A. C., Muthukrishnan, S. D. and Oxburgh, L. (2015). A synthetic niche for nephron progenitor cells. *Dev. Cell* **34**, 229-241. doi:10.1016/j.devcel.2015.06.021

Brunskill, E. W., Park, J.-S., Chung, E., Chen, F., Magella, B. and Potter, S. S. (2014). Single cell dissection of early kidney development: multilineage priming. *Development* **141**, 3093-3101. doi:10.1242/dev.110601

Carroll, T. J., Park, J.-S., Hayashi, S., Majumdar, A. and McMahon, A. P. (2005). Wnt9b plays a central role in the regulation of mesenchymal to epithelial transitions underlying organogenesis of the mammalian urogenital system. *Dev. Cell* **9**, 283-292. doi:10.1016/j.devcel.2005.05.016

Chen, X., Hou, X.-M., Fan, Y.-F., Jin, Y.-T. and Wang, Y.-L. (2016). Sonic hedgehog protein regulates fibroblast growth factor 8 expression in metanephric explant culture from BALB/c mice: Possible mechanisms associated with renal morphogenesis. *Mol. Med. Rep.* **14**, 2929-2936. doi:10.3892/mmr.2016.5614

Clements, D., Taylor, H. C., Herrmann, B. G. and Stott, D. (1996). Distinct regulatory control of the brachyury gene in axial and non-axial mesoderm suggests separation of mesoderm lineages early in mouse gastrulation. *Mech. Dev.* **56**, 139-149. doi:10.1016/0925-4773(96)00520-5

Combes, A. N., Lefevre, J. G., Wilson, S., Hamilton, N. A. and Little, M. H. (2016). Cap mesenchyme cell swarming during kidney development is influenced by attraction, repulsion, and adhesion to the ureteric tip. *Dev. Biol.*, **418**, 297-306. doi:10.1016/j.ydbio.2016.06.028

Costantini, F. and Kopan, R. (2010). Patterning a complex organ: branching morphogenesis and nephron segmentation in kidney development. *Dev. Cell* **18**, 698-712. doi:10.1016/j.devcel.2010.04.008

Dapkunas, A., Rantanen, V., Gui, Y., Lalowski, M., Sainio, K., Kuure, S. and Sariola, H. (2019). Simple 3d culture of dissociated kidney mesenchyme mimics nephron progenitor niche and facilitates nephrogenesis wnt-independently. *Sci. Rep.* **9**, 13433. doi:10.1038/s41598-019-49526-x

Das, A., Tanigawa, S., Karner, C. M., Xin, M., Lum, L., Chen, C., Olson, E. N., Perantoni, A. O. and Carroll, T. J. (2013). Stromal–epithelial crosstalk regulates kidney progenitor cell differentiation. *Nat. Cell Biol.* **15**, 1035. doi:10.1038/ncb2828

Davies, J. (2016). 11 - The Urinary System. In *Kaufman's Atlas of Mouse Development Supplement* (ed. R. Baldock, J. Bard, D. R. Davidson and G. Morriss-Kay), pp. 139-146. Boston: Academic Press.

Diehn, B., Feinleib, M., Haupt, W., Hildebrand, E., Lenci, F. and Nultsch, W. (1977). Terminology of behavioral responses of motile microorganisms. *Photochem. Photobiol.* **26**, 559-560. doi:10.1111/j.1751-1097.1977.tb07532.x

Fic, E., Kedracka-Krok, S., Jankowska, U., Pirog, A. and Dziedzicka-Wasylewska, M. (2010). Comparison of protein precipitation methods for various rat brain structures prior to proteomic analysis. *Electrophoresis* **31**, 3573-3579. doi:10.1002/elps.201000197

Grieshammer, U., Cebrián, C., Ilagan, R., Meyers, E., Herzlinger, D. and Martin, G. R. (2005). Fgf8 is required for cell survival at distinct stages of nephrogenesis and for regulation of gene expression in nascent nephrons. *Development* **132**, 3847-3857. doi:10.1242/dev.01944

Harding, S. D., Armit, C., Armstrong, J., Brennan, J., Cheng, Y., Haggarty, B., Houghton, D., Lloyd-MacGilp, S., Pi, X., Roochun, Y. et al. (2011). The gudmap database–an online resource for genitourinary research. *Development* **138**, 2845-2853. doi:10.1242/dev.063594

Huh, S.-H., Ha, L. and Jang, H.-S. (2020). Nephron progenitor maintenance is controlled through fibroblast growth factors and sprouty1 interaction. *J. Am. Soc. Nephrol.* **31**, 2559-2572. doi:10.1681/ASN.2020040401

Ihermann-Hella, A., Hirashima, T., Kupari, J., Kurtzeborn, K., Li, H., Kwon, H. N., Cebrian, C., Soofi, A., Dapkunas, A., Miinalainen, I. et al. (2018). Dynamic mapk/erk activity sustains nephron progenitors through niche regulation and primes precursors for differentiation. *Stem Cell Rep.* **11**, 912-928. doi:10.1016/j.stemcr.2018.08.012

Junttila, S., Saarela, U., Halt, K., Manninen, A., Pärssinen, H., Lecca, M. R., Brändli, A. W., Sims-Lucas, S., Skovorodkin, I. and Vainio, S. J. (2015). Functional genetic targeting of embryonic kidney progenitor cells ex vivo. *J. Am. Soc. Nephrol.* **26**, 1126-1137. doi:10.1681/ASN.2013060584

Katoh, M. and Katoh, M. (2006). Cross-talk of wnt and fgf signaling pathways at gsk3ß to regulate ß-catenin and snail signaling cascades. *Cancer Biol. Ther.* **5**, 1059-1064. doi:10.4161/cbt.5.9.3151

Kispert, A., Vainio, S., Shen, L., Rowitch, D. H. and McMahon, A. P. (1996). Proteoglycans are required for maintenance of Wnt-11 expression in the ureter tips. *Development* **122**, 3627-3637. doi:10.1242/dev.122.11.3627

Kobayashi, A., Kwan, K.-M., Carroll, T. J., McMahon, A. P., Mendelsohn, C. L. and Behringer, R. R. (2005). Distinct and sequential tissue-specific activities of the lim-class homeobox gene lim1 for tubular morphogenesis during kidney development. *Development* **132**, 2809-2823. doi:10.1242/dev.01858

Kobayashi, A., Valerius, M. T., Mugford, J. W., Carroll, T. J., Self, M., Oliver, G. and McMahon, A. P. (2008). Six2 defines and regulates a multipotent selfrenewing nephron progenitor population throughout mammalian kidney development. *Cell Stem Cell* **3**, 169-181. doi:10.1016/j.stem.2008.05.020

Krishnan Harish, R., Gupta, M., Zoller, D., Hartmann, H., Gheisari, A., Machate, A., Hans, S. and Brand, M. (2022). Real-time monitoring of endogenous Fgf8a gradient attests to its role as a morphogen during zebrafish gastrulation. Technical report, *bioRxiv*. https://www.biorxiv.org/content/10.1101/2022.04.26.488902v1.

Kuure, S. and Sariola, H. (2020). Mouse models of congenital kidney anomalies. *Animal Model. Hum. Birth Defect.* **1236**, 109-136. doi:10.1007/978-981-15-2389-2_5

Lawlor, K. T., Zappia, L., Lefevre, J., Park, J.-S., Hamilton, N. A., Oshlack, A., Little, M. H. and Combes, A. N. (2019). Nephron progenitor commitment is a stochastic process influenced by cell migration. *eLife* **8**, e41156. doi:10.7554/eLife.41156

Li, Z., Araoka, T., Wu, J., Liao, H.-K., Li, M., Lazo, M., Zhou, B., Sui, Y., Wu, M.-Z., Tamura, I. et al. (2016). 3d culture supports long-term expansion of mouse and human nephrogenic progenitors. *Cell Stem Cell* **19**, 516-529. doi:10.1016/j.stem.2016.07.016

Li, H., Hohenstein, P. and Kuure, S. (2021). Embryonic kidney development, stem cells and the origin of wilms tumor. *Genes* **12**, 318. doi:10.3390/genes12020318

Lin, Y., Zhang, S., Rehn, M., Itaranta, P., Tuukkanen, J., Heljasvaara, R., Peltoketo, H., Pihlajaniemi, T. and Vainio, S. (2001). Induced repatterning of type xviii collagen expression in ureter bud from kidney to lung type: association with sonic hedgehog and ectopic surfactant protein c. *Development* **128**, 1573-1585. doi:10.1242/dev.128.9.1573

Lindström, N. O., De Sena Brandine, G., Tran, T., Ransick, A., Suh, G., Guo, J., Kim, A. D., Parvez, R. K., Ruffins, S. W., Rutledge, E. A. et al. (2018a). Progressive recruitment of mesenchymal progenitors reveals a time-dependent process of cell fate acquisition in mouse and human nephrogenesis. *Dev. Cell* **45**, 651-660.e4. doi:10.1016/j.devcel.2018.05.010

Lindström, N. O., Tran, T., Guo, J., Rutledge, E., Parvez, R. K., Thornton, M. E., Grubbs, B., McMahon, J. A. and McMahon, A. P. (2018b). Conserved and divergent molecular and anatomic features of human and mouse nephron patterning. *J. Am. Soc. Nephrol.* **29**, 825-840. doi:10.1681/ASN.2017091036

Liu, H., Chen, S., Yao, X., Li, Y., Chen, C.-H., Liu, J., Saifudeen, Z. and El-Dahr, S. S. (2018). Histone deacetylases 1 and 2 regulate the transcriptional programs of nephron progenitors and renal vesicles. *Development* **145**, dev153619. doi:10.1242/dev.153619

Makarenkova, H. P., Hoffman, M. P., Beenken, A., Eliseenkova, A. V., Meech, R., Tsau, C., Patel, V. N., Lang, R. A. and Mohammadi, M. (2009). Differential interactions of FGFs with Heparan sulfate control gradient formation and branching morphogenesis. *Sci. Signal.* **2**, ra55. doi:10.1126/scisignal.2000304

Mari, C. and Winyard, P. (2015). Concise review: understanding the renal progenitor cell niche in vivo to recapitulate nephrogenesis in vitro. *Stem Cell. Transl. Med.* **4**, 1463-1471. doi:10.5966/sctm.2015-0104

Mathew, S., Chen, X., Pozzi, A. and Zent, R. (2012). Integrins in renal development. *Pediatr. Nephrol.* **27**, 891-900. doi:10.1007/s00467-011-1890-1

Matsuo, I. and Kimura-Yoshida, C. (2014). Extracellular distribution of diffusible growth factors controlled by heparan sulfate proteoglycans during mammalian embryogenesis. *Philos. Trans. R. Soc. B Biol. Sci.* **369**, 20130545. doi:10.1098/rstb.2013.0545

Meyers, E. N., Lewandoski, M. and Martin, G. R. (1998). An fgf8 mutant allelic series generated by cre- and flp-mediated recombination. *Nat. Genet.* **18**, 136. doi:10.1038/ng0298-136

Mokhtari, Z., Mech, F., Zitzmann, C., Hasenberg, M., Gunzer, M. and Figge, M. T. (2013). Automated characterization and parameter-free classification of cell tracks based on local migration behavior. *PLoS ONE* **8**, e80808. doi:10.1371/journal.pone.0080808

Mugford, J. W., Sipilä, P., McMahon, J. A. and McMahon, A. P. (2008). Osr1 expression demarcates a multi-potent population of intermediate mesoderm that undergoes progressive restriction to an osr1-dependent nephron progenitor compartment within the mammalian kidney. *Dev. Biol.* **324**, 88-98. doi:10.1016/j.ydbio.2008.09.010

Mugford, J. W., Yu, J., Kobayashi, A. and McMahon, A. P. (2009). High-resolution gene expression analysis of the developing mouse kidney defines novel cellular compartments within the nephron progenitor population. *Dev. Biol.* **333**, 312-323. doi:10.1016/j.ydbio.2009.06.043

Munro, D. A. D., Hohenstein, P. and Davies, J. A. (2017). Cycles of vascular plexus formation within the nephrogenic zone of the developing mouse kidney. *Sci. Rep.* **7**, 3273. doi:10.1038/s41598-017-03808-4

Muzumdar, M. D., Tasic, B., Miyamichi, K., Li, L. and Luo, L. (2007). A global double-fluorescent cre reporter mouse. *Genesis* **45**, 593-605. doi:10.1002/dvg.20335

O'Brien, L. L. (2019). Nephron progenitor cell commitment: Striking the right balance. *Semin. Cell Dev. Biol.* **91**, 94-103. doi:10.1016/j.semcdb.2018.07.017

O'Brien, L. L., Combes, A. N., Short, K. M., Lindström, N. O., Whitney, P. H., Cullen-McEwen, L. A., Ju, A., Abdelhalim, A., Michos, O., Bertram, J. F. et al. (2018). Wnt11 directs nephron progenitor polarity and motile behavior ultimately determining nephron endowment. *Elife* **7**, e40392. doi:10.7554/eLife.40392

Oxburgh, L. (2018). Kidney nephron determination. *Annu. Rev. Cell Dev. Biol.* **34**, 427-450. doi:10.1146/annurev-cellbio-100616-060647

Perantoni, A. O., Dove, L. F. and Karavanova, I. (1995). Basic fibroblast growth factor can mediate the early inductive events in renal development. *Proc. Natl Acad. Sci. USA* **92**, 4696-4700. doi:10.1073/pnas.92.10.4696

Perantoni, A. O., Timofeeva, O., Naillat, F., Richman, C., Pajni-Underwood, S., Wilson, C., Vainio, S., Dove, L. F. and Lewandoski, M. (2005). Inactivation of fgf8 in early mesoderm reveals an essential role in kidney development. *Development* **132**, 3859-3871. doi:10.1242/dev.01945

Pileri, S. A., Roncador, G., Ceccarelli, C., Piccioli, M., Briskomatis, A., Sabattini, E., Ascani, S., Santini, D., Piccaluga, P. P., Leone, O. et al. (1997). Antigen retrieval techniques in immunohistochemistry: comparison of different methods. *J. Pathol.* **183**, 116-123. doi:10.1002/(SICI)1096-9896(199709)183:1<116::AID-PATH1087>3.0.CO;2-2

R Core Team. (2020). *R: A Language and Environment for Statistical Computing*. Vienna, Austria: R Foundation for Statistical Computing. https://www.R-project.org/.

Reginensi, A., Scott, R. P., Gregorieff, A., Bagherie-Lachidan, M., Chung, C., Lim, D.-S., Pawson, T., Wrana, J. and McNeill, H. (2013). Yap-and cdc42-dependent nephrogenesis and morphogenesis during mouse kidney development. *PLoS Genet.* **9**, e1003380. doi:10.1371/journal.pgen.1003380

Ribatti, D. and Santoiemma, M. (2014). Epithelial-mesenchymal interactions: a fundamental developmental biology mechanism. *Int. J. Dev. Biol.* **58**, 303-306. doi:10.1387/ijdb.140143dr

Scarpa, E. and Mayor, R. (2016). Collective cell migration in development. *J. Cell Biol.* **212**, 143-155. doi:10.1083/jcb.201508047

SenGupta, S., Parent, C. A. and Bear, J. E. (2021). The principles of directed cell migration. *Nat. Rev. Mol. Cell Biol.* **22**, 529-547. doi:10.1038/s41580-021-00366-6

Shan, J., Jokela, T., Skovorodkin, I. and Vainio, S. (2010). Mapping of the fate of cell lineages generated from cells that express the wnt4 gene by time-lapse during kidney development. *Differentiation* **79**, 57-64. doi:10.1016/j.diff.2009.08.006

Soriano, P. (1999). Generalized lacz expression with the rosa26 cre reporter strain. *Nat. Genet.* **21**, 70-71. doi:10.1038/5007

Stapornwongkul, K. S. and Vincent, J.-P. (2021). Generation of extracellular morphogen gradients: the case for diffusion. *Nat. Rev. Genet.* **22**, 393-411. doi:10.1038/s41576-021-00342-y

Stark, K., Vainio, S., Vassileva, G. and McMahon, A. P. (1994). Epithelial transformation of metanephric mesenchyme in the developing kidney regulated by wnt-4. *Nature* **372**, 679. doi:10.1038/372679a0

Sun, X., Meyers, E. N., Lewandoski, M. and Martin, G. R. (1999). Targeted disruption of fgf8 causes failure of cell migration in the gastrulating mouse embryo. *Genes Dev.* **13**, 1834-1846. doi:10.1101/gad.13.14.1834

Tanaka, S., Sichau, D. and Iber, D. (2015). LBIBCell: a cell-based simulation environment for morphogenetic problems. *Bioinformatics* **31**, 2340-2347. doi:10.1093/bioinformatics/btv147

Tanigawa, S., Taguchi, A., Sharma, N., Perantoni, A. O. and Nishinakamura, R. (2016). Selective in vitro propagation of nephron progenitors derived from embryos and pluripotent stem cells. *Cell Rep.* **15**, 801-813. doi:10.1016/j.celrep.2016.03.076

Tikka, P., Mercker, M., Skovorodkin, I., Saarela, U., Vainio, S., Ronkainen, V.-P., Sluka, J. P., Glazier, J. A., Marciniak-Czochra, A. and Schaefer, F. (2022). Computational modelling of nephron progenitor cell movement and aggregation during kidney organogenesis. *Math Biosci.* **344**, 108759. doi:10.1016/j.mbs.2021.108759

Trueb, B. (2011). Biology of fgfrl1, the fifth fibroblast growth factor receptor. *Cell. Mol. Life Sci.* **68**, 951-964. doi:10.1007/s00018-010-0576-3

Uchiyama, Y., Sakaguchi, M., Terabayashi, T., Inenaga, T., Inoue, S., Kobayashi, C., Oshima, N., Kiyonari, H., Nakagata, N., Sato, Y. et al. (2010). Kif26b, a kinesin family gene, regulates adhesion of the embryonic kidney mesenchyme. *Proc. Natl Acad. Sci. USA* **107**, 9240-9245. doi:10.1073/pnas.0913748107

Veikkolainen, V., Naillat, F., Railo, A., Chi, L., Manninen, A., Hohenstein, P., Hastie, N., Vainio, S. and Elenius, K. (2012). Erbb4 modulates tubular cell polarity and lumen diameter during kidney development. *J. Am. Soc. Nephrol.* **23**, 112-122. doi:10.1681/ASN.2011020160

Walker, K. A., Sims-Lucas, S. and Bates, C. M. (2016). Fibroblast growth factor receptor signaling in kidney and lower urinary tract development. *Pediatr. Nephrol.* **31**, 885-895. doi:10.1007/s00467-015-3151-1

Wortel, I. M. N., Liu, A. Y., Dannenberg, K., Berry, J. C., Miller, M. J. and Textor, J. (2021). CelltrackR: An R package for fast and flexible analysis of immune cell migration data. *ImmunoInformatics* **1-2**, 100003. doi:10.1016/j.immuno.2021.100003

Xu, J., Liu, H., Park, J.-S., Lan, Y. and Jiang, R. (2014). Osr1 acts downstream of and interacts synergistically with six2 to maintain nephron progenitor cells during kidney organogenesis. *Development* **141**, 1442-1452. doi:10.1242/dev.103283

Yan, D. and Lin, X. (2009). Shaping morphogen gradients by proteoglycans. *Cold Spring Harbor Perspect. Biol.*, **1**, a002493. doi:10.1101/cshperspect.a002493. http://cshperspectives.cshlp.org/content/1/3/a002493. Company: Cold Spring Harbor Laboratory Press Distributor: Cold Spring Harbor Laboratory Press Institution: Cold Spring Harbor Laboratory Press Label: Cold Spring Harbor Laboratory Press Publisher: Cold Spring Harbor Lab.

Yu, J., Carroll, T. J. and McMahon, A. P. (2002). Sonic hedgehog regulates proliferation and differentiation of mesenchymal cells in the mouse metanephric kidney. *Development* **129**, 5301-5312. doi:10.1242/dev.129.22.5301

Yu, S. R., Burkhardt, M., Nowak, M., Ries, J., Petrášek, Z., Scholpp, S., Schwille, P. and Brand, M. (2009). Fgf8 morphogen gradient forms by a source-sink mechanism with freely diffusing molecules. *Nature* **461**, 533. doi:10.1038/nature08391

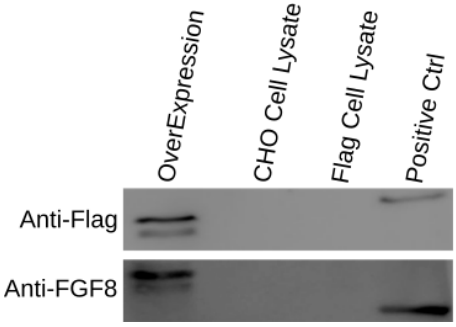

Fig. S1. The specificity of the FGF8 antibody. Western blot assay revealed the specificity of FGF8 antibody using flag-tagged FGF8 construct expressed in CHO cells. The positive control was FGF8b recombinant protein which gave a 23 kDa band. The over-expressed flag-tagged FGF8 protein in CHO cells had a higher molecular weight (˜30 KD) as compared to the control. FGF8 contains glycosylated sites and the FGF8b protein produced in CHO cells has different post-translation modifications compared to the control produced in *E. Coli.* The variation in molecular weight between both samples is attributed to the presence of different glycan profiles. The flag tag was observed in the overexpressed flag-tagged FGF8 cell line.

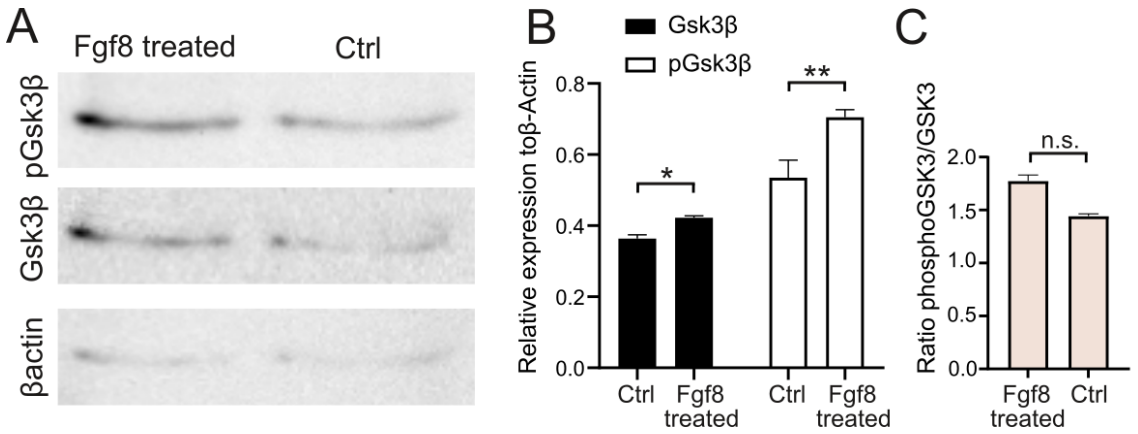

Fig. S2. Expression of *GSK3β* in response to Fgf8b. (A) Western blot analysis of phospho-*GSK3β* production in response to ectopic FGF8b in nephrosphere culture. (B) Relative expression of *GSK3β* and phospho-*GSK3β*. Statistics were performed (n=3) using Two-way ANOVA. **p < 0.023 and *p < 0.028. (C) Ratio of phospho-*GSK3β* on *GSK3β* showed no statistical difference between the treated ectopic FGF8b and the control nephrosphere.

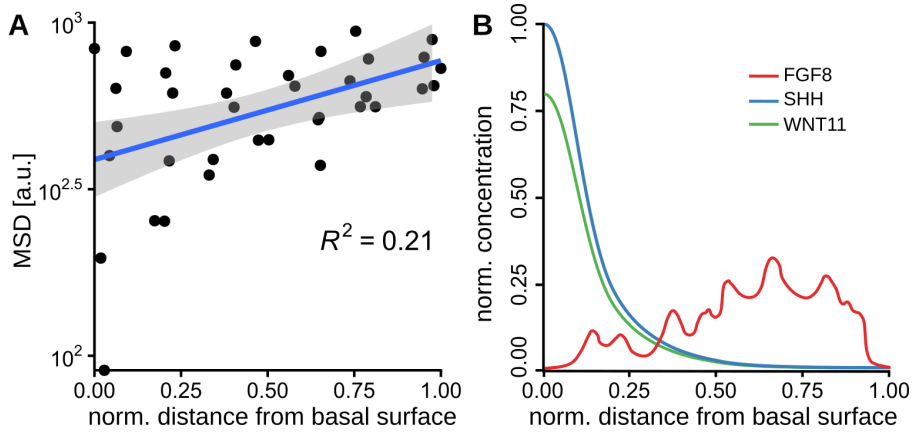

Fig. S3. Simulated motility and concentration gradients. (A) The observed motility gradient in the simulations quantified by the mean squared displacement (MSD) of each NPC from its initial position with respect to the distance from the basal surface of the ureteric epithelium. Each dot represents the average over n=20 simulations of the squared displacement of each NPC from the same initial position. The blue solid line and shadowed region represent a linear regression with confidence interval (95% confidence level). The low coefficient of determination R^2 indicates the variability of NPC displacements, reflecting the randomness of NPC motility. (B) Example of concentration profiles in the simulations. Curves represent concentration profiles along a line perpendicular to the basal surface of the ureteric epithelium. Concentrations were normalized to the maximum SHH concentration.

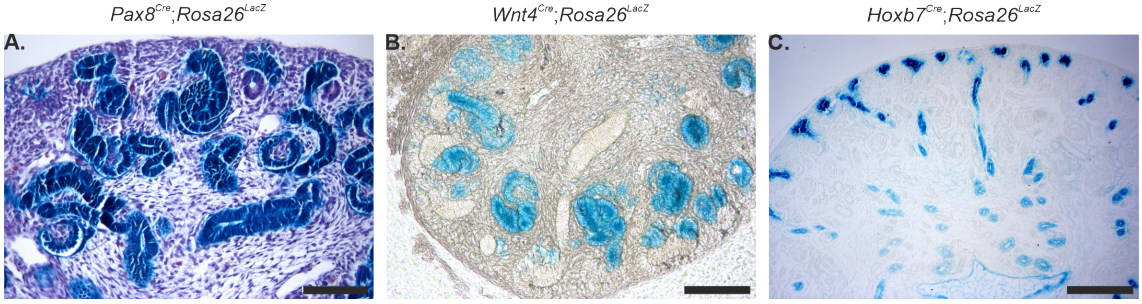

Fig. S4. X-gal staining after *β* − Galactosidase expression due to Cre recombination. (A) E14.5 *Pax8*^{Cre}, (B) W *nt4*^{Cre} and (C) E16.5 *Hoxb7*^{Cre} mouse kidneys. (A) Expression of PAX8 is limited to the UB tip and MM. (B) WNT4 expression is observed in pretubular aggregates (PTAs). (C) HOXb7 expression is limited to the UB and no expression was observed in the MM. Scale bar represents 100 μm.

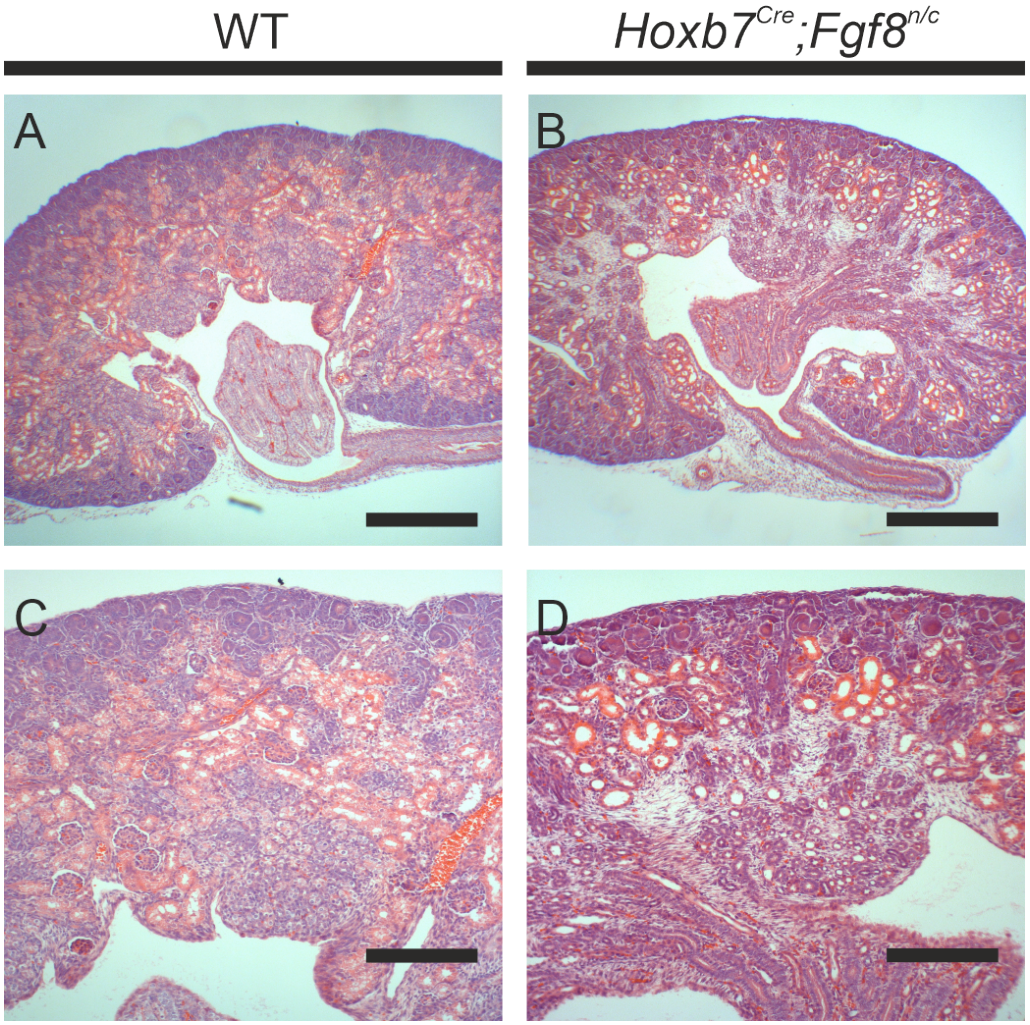

Fig. S5. Hematoxylin-Eosin staining of (A-C) littermate control (WT) and (B-D) *Fgf8* $^{n/c}$;*Hoxb7* ^{Cre} shows no phenotype. Scale bar represents 100 μm.

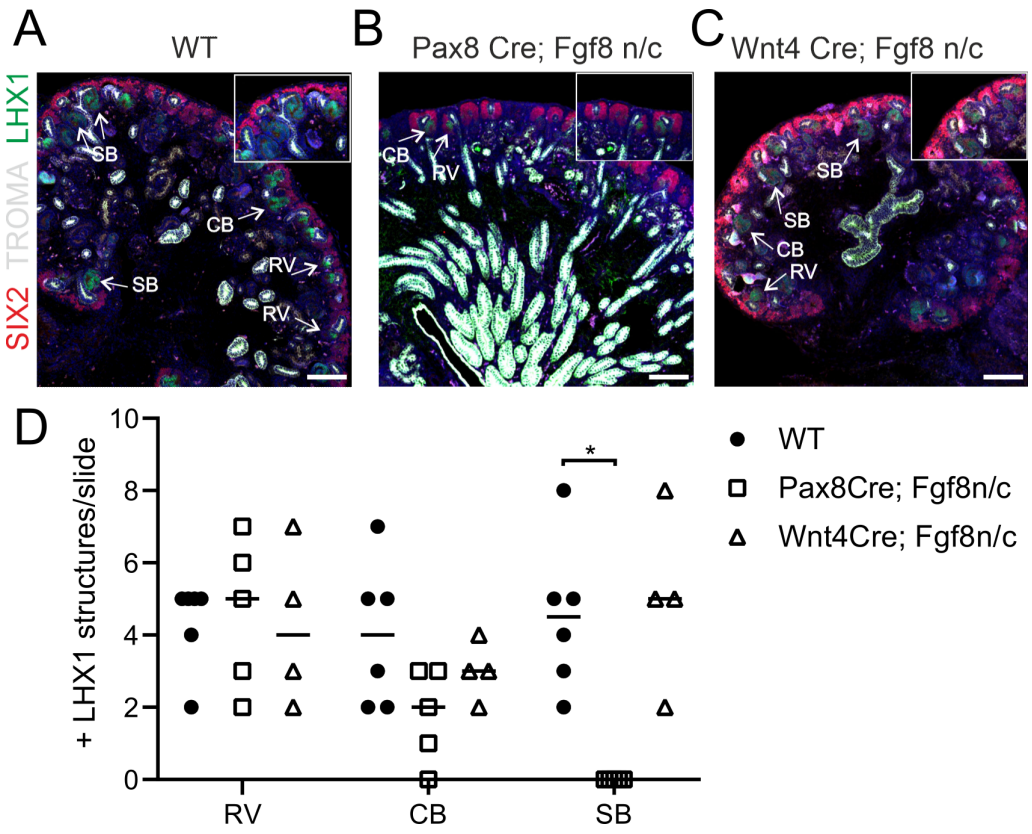

Fig. S6. Staining and quantification of LHX1 positive structures in *Fgf8*$^{n/c}$; *Pax8*^{Cre} and *Fgf8*$^{n/c}$;*Wnt4*^{Cre} kidneys. (A-C) Immunostaining for SIX2, LHX1 and TROMA1 counter-stained with Hoechst showing reduced LHX1 expression in nascent nephrons of *Fgf8*$^{n/c}$; *Pax8*^{Cre} kidneys compared with the wildtype (WT) and *Fgf8*$^{n/c}$;*Wnt4*^{Cre} mutant kidneys. The inserts are higher magnification selections. Scale bars represent 100 µm. (D) Quantification of the positive identified LHX1 structures. (RV) renal vesicle, (CB) comma-shaped body, (SB) S-shaped body. Statistical test was performed based on two-way ANOVA Sidak multiple comparison with significance level *p <0.01.

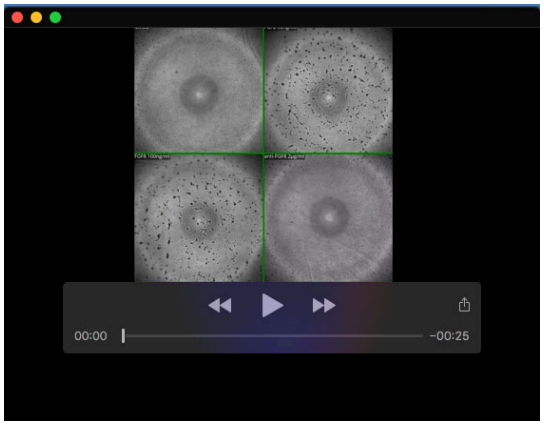

Movie 1. 24-hour time lapse imaging of *in vitro* experiments where NPCs were cultured in a 3D matrix. (A) NPCs cultured without any additive (control), (B) NPCs cultured in FGF2, (C) NPCs cultured in FGF8 and (D) NPCs cultured in anti-FGF8b antibody. Scale bar represents 50 µm. https://git.bsse.ethz.ch/iber/Publications/2022_Meer_NPC_Condensation/-/blob/main/Video1 spherification montage.mp4.

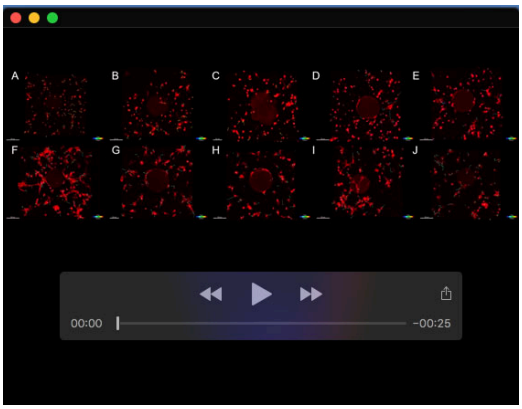

Movie 2. Time lapse imaging of in vitro experiments with control beads (A-E) vs. FGF8 soaked beads (F-J), 5 samples each. Dragon tails are shown.
Scale bars: 50 µm. https://git.bsse.ethz.ch/iber/Publications/2022_Meer_NPC_Condensation/-/blob/main/Video2cellmotility quant.mp4.

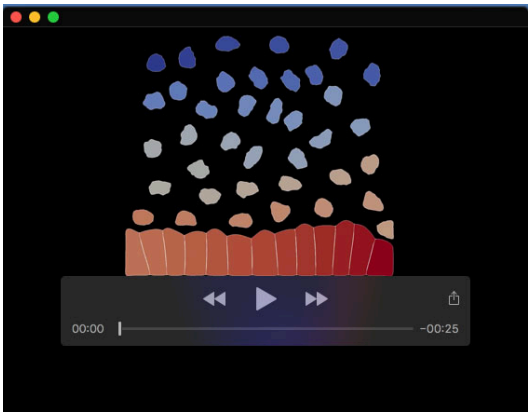

Movie 3. Simulations of increasing relative FGF8 concentrations: Weak, intermediate (twofold increase) and high (threefold increase). https://git.bsse.ethz.ch/iber/Publications/2022_Meer_NPC_Condensation/-/blob/main/Video3 mesenchymal condensation simulations.mp4.

Table S1. Mouse lines used in this work

Reagent type (Species)	Designation	Source or reference	Identifiers
Genetic reagent (Mus musculus)	*Pax8*$^{Cre/+}$	(Bouchard et al., 2002)	MGI:J:80208
Genetic reagent (Mus musculus)	*Wnt4*$^{eGFPCre/+}$	(Shan et al., 2010)	RRID:IMSR EM:10011
Genetic reagent (Mus musculus)	*Hoxb7*$^{Cre/+}$	(Yu et al., 2002)	MGI:J:79481
Genetic reagent (Mus musculus)	*Fgf8* $^{Floxed/Floxed}$	(Meyers et al., 1998)	MG:2150347
Genetic reagent (Mus musculus)	*Fgf8* $^{\Delta 2,3/+}$	(Meyers et al., 1998)	MGI:2150346
Genetic reagent (Mus musculus)	*T*$^{Cre/+}$	(Perantoni et al., 2005)	MGI:J:101175
Genetic reagent (Mus musculus)	*Rosa26*$^{mT/mG}$	(Muzumdar et al., 2007)	MGI:J:124702
Genetic reagent (Mus musculus)	*Six2−TGC*^{tg}	(Kobayashi et al., 2008)	MGI:J:148455
Genetic reagent (Mus musculus)	*Rosa26−LacZ*^{loxP}	(Soriano, 1999)	MGI:J:64292

Table S2. Antibodies, growth factors, agonists and antagonists

Product	Incubation Temperature; Time	Final Concentration	Company; Catalogue number; Identifiers
Anti-SIX2	+4°C; Overnight	1:200	Proteintech Group; Cat# 11562-1-AP;RRID:AB_2189084
Anti-PAX2	+4°C; Overnight	1:200	BioLegend; Cat# 901001; RRID:AB_2565001
Anti-FGF8b	+4°C; Overnight	1:200	RD Systems; Cat# AF-423-NA; RRID:AB_2262650
Anti-Flag M2	RT; 1 hr	1:300	Sigma-Aldrich; Cat# F1804; RRID:AB_262044
Anti-TROMA1	+4°C; Overnight	1:200	DSHB; Cat# Troma1; RRID:AB_531826
Anti-LHX1	+4°C; Overnight	1:200	DSHB; Cat# 4F2; RRID:AB_531784
Anti-GSK3β	+4°C; Overnight	1:1000	Cell Signalling; Cat#9315S; RRID:AB_490890
Anti-phospho-GSK3β	+4°C; Overnight	1:1000	Cell Signalling; Cat#9336S; RRID:AB_331405
Anti-β-ACTIN	+4°C; Overnight	1:1000	Cell Signalling; Cat#4970S; RRID:AB_2223172
Goat anti-Rabbit	RT; 1 h	1:1000	ThermoFisher Scientific; Cat# A-11008;
AlexaFluor488			RRID:AB_143165
Goat anti-Rat	RT; 1 h	1:1000	ThermoFisher Scientific; Cat# A-11081;
AlexaFluor546			RRID:AB_2534125
Goat anti-Rabbit	RT; 1 h	1:1000	AgilentDako; Cat# P0448;
HRP			RRID:AB_2617138
rmFGF8b		100 ng/µl	RD Systems; Cat# 423-NA
PP2		10 µM	Tocris Bioscience; Cat# 1407; PubChem ID: 4878
Bio		10 µM	Torcis Bioscience; Cat# 3194; PubChem ID: 5287844
Matrigel (BME)			Corning;

Table S3. qPCR primers

Gene Target	Sequence 5'→ 3'
Six2	AGGAAAGGGAGAACAGCGAGAA
	GGACTGGACGACGAGTGGT
Eya1	AATTTATGCCTGGCAACTGG
	CAGACCTCCCACGTTGTTTT
Cited2	TGCAGAAGCTCAACAACCAG
	CTGGTTTGTCCCGTTCATCT
Sall1	AGCCTCAACATTTCCAATCC
	TGGGCATCCTTGCTCTTAGT
Wnt9b	TGGCTTTCGTGAGCATGGAG
	AAAGACAGCCACGGTGTGGTAA
Fgf8	TGTTGCACTTGCTGGTTCTC
	CGGCTGTAGAGCTGGTAGG
Lim1(Lhx1)	CAGTGTCGCCAAAGAGAACA
	TGAGACGTTGGCACTTTCAG
Wnt4	CTGGAGAAGTGTGGCTGTGA
	GGACGTCCACAAAGGACTGT
GAPDH	AGAACATCATCCCTGCATCC
	CAGTGAGCTTCCCGTTCAG

Table S4. Parameter values

Solver	Parameter description	Value [LB units]	Value [SI units]
Cell Growth	BioSolver application rate	1:1	
	mass source strength	$6 \cdot 10^{-6}$	N/A
Cell Boundary Tension	BioSolver application rate	1:10	
	Hookean spring constant UB|NPCs	$10^{-3} \mid 5 \cdot 10^{-4}$	N/A
Cell Junction	BioSolver application rate	1:10	
	junction search radius UB|NPCs	1.0|2.0	0.5 µm|1 µm
	intercellular junction length	0.3	0.15 µm
	Hookean spring constant UB|NPCs	$10^{-2} \mid 10^{-3}$	N/A
Cell Motility (Fgf8)	BioSolver application rate	1:1	
	normal velocity dist. $\mathcal{N}(0,\sigma)$	$\sigma = [Fgf8]_{cell} 10^{-3}$	$\{1,\ldots,10\} \frac{\mu m}{h}$
Cell Motility (Wnt11)	BioSolver application rate	1:1	
	uniform velocity dist. $p(x\|0,b)$	$b = [Wnt11]_{cell} 10^{-4}$	$\{0.1,\ldots,1\} \frac{\mu m}{h}$
Fgf8	CDESolver application rate	1:1	
	diffusion coefficient D_{Fgf8}	$\tau = 2.0$	$0.579 \frac{\mu m^2}{s}$
	production rate ρ_{Fgf8}	$\frac{\{2,3,4\} \cdot 10^{-3}}{\text{iteration}}$	$\{6.9,13.9,74.1\} \frac{10^{-3}}{s}$

Solver	Parameter description	Value [LB units]	Value [SI units]
	degradation rate δ_{Fgf8}	$\frac{10^{-3}}{\text{iteration}}$	$4.6\frac{10^{-3}}{s}$
	gradient length λ_{Fgf8}	22.44	11.22 µm
	repression H^{S-}	$1/\left(1+\left(\frac{[SHH]}{100}\right)^{2}\right)$	N/A
SHH	CDESolver application rate	1:1	
	diffusion coefficient D_{SHH}	$\tau = 2.0$	$0.579\frac{\mu m^{2}}{s}$
	production rate ρ_{SHH}	$\frac{2\cdot10^{-3}}{\text{iteration}}$	$9.3\frac{10^{-3}}{s}$
	degradation rate δ_{SHH}	$\frac{5\cdot10^{-4}}{\text{iteration}}$	$2.3\frac{10^{-3}}{s}$
	gradient length λ_{SHH}	31.74	15.87 µm
Wnt11	CDESolver application rate	1:1	
	diffusion coefficient D_{Wnt11}	$\tau = 2.0$	$0.579\frac{\mu m^{2}}{s}$
	production rate ρ_{Wnt11}	$\frac{2\cdot10^{-3}}{\text{iteration}}$	$9.3\frac{10^{-3}}{s}$
	degradation rate δ_{Wnt11}	$\frac{5\cdot10^{-4}}{\text{iteration}}$	$2.3\frac{10^{-3}}{s}$
	gradient length λ_{Wnt11}	31.74	15.87 µm